UNIVERSITY OF CALIFORNIA,
IRVINE

Residential Demand Response: Generation, Storage, and Load Management

DISSERTATION

submitted in partial satisfaction of the requirements
for the degree of

DOCTOR OF PHILOSOPHY

in Electrical Engineering and Computer Science

by

Nadia Ahmed

Dissertation Committee:
Professor Marco Levorato, Chair
Professor G.P. Li
Professor Knut Sølna
Professor Michael Green

2017

DEDICATION

To the sacrifice.

TABLE OF CONTENTS

LIST OF FIGURES

LIST OF TABLES

ACKNOWLEDGMENTS

I would like to thank Howard G. Tucker, the first student of David Blackwell and prodigy of Jerzy Neyman, who I've spent many walks around ring road discussing politics, the McCarthy era, dynamic programming, and σ algebras with. You have been an inspiration to me and have always encouraged me to "Never give up, coraggio!"

I would also like to thank Knut Sølna who has spent weekends welcoming my questions. Prof. Sølna never wastes his words and only speaks substance! Amelia Regan has also been a wonderful friend and advocate. Throughout this journey, she held an open door policy and is always available to give advice or listen when I am down. Kumar Wickramasinghe has been instrumental in helping me track my progress and set up a criteria and timeline to propel me towards my goals. He has taught me valuable organizational lessons as well as demonstrated to me a deep appreciation and respect for all people and students. I would also like to thank Patrick Guidotti for spending time with me after the Applied Math seminar series helping me improve my mathematical communication skills as well as teaching me that simple is always better.

I cannot go without thanking the late Rui de Figueiredo, my original graduate thesis advisor who passed July 22, 2013. Though he was very strict, he pushed the limits in terms of research and was constantly learning and willing to try new things. He also cared very deeply about his students, and while he worked us hard, he also appreciated our presence in his life. I would also like to thank Nancy Ruyter who taught me to keep writing and not fear criticism but to welcome it. I'd like to thank Tong Wang, Diane Diefenderfer, Shawn Boyle d'Arcy, and Molly Lynch for teaching me that discipline and work ethic applies to all parts of life.

I would like to acknowledge the contributions of Roberto Valentini who has been a friend and overall class person. He is always open to help without judgement and a positive attitude. I would like to to thank Marco Levorato for giving me a hell of a ride, providing me an engaging problem to solve, and pushing me to the do things I didn't know I was capable of. To GP Li, I thank you for continuing to work with me towards my degree.

I also would like to acknowledge IEEE Transactions on Smart Grid who have given me permission to incorporate the work I've done into my dissertation.

Lastly, I would like to thank love for keeping me going. You have stayed up late nights with me, helped me when I was in pain, saved me when I was hopeless, hugged me when I felt alone. You manifested yourself in unusual ways, in my daily life, in my friends, in my family, in my sacrifice, and in my heart. You hurt me and strengthened me at the worst and best of times. You are my purpose.

CURRICULUM VITAE

Nadia Ahmed

EDUCATION

Doctor of Philosophy in Electrical Engineering & Computer Science **2017**
University of California, Irvine *Irvine, CA*

Masters of Science in Electrical Engineering & Computer Science **2007**
University of California, Irvine *Irvine, CA*

Bachelor of Science in Electrical Engineering & Computer Science **2005**
University of California, Irvine *Irvine, CA*

TEACHING EXPERIENCE

Associate Professor of Computer Science **Jan 2014 – May 2018**
Saddleback College *Mission Viejo, CA*

Instructor of Computer Science **Jan 2017– May 2018**
Orange Coast College *Costa Mesa, CA*

Teaching Assistant **Sept 2005 – June 2017**
University of California, Irvine *Irvine, CA*

REFEREED JOURNAL PUBLICATIONS

Residential Consumer-Centric Demand Side Management **2017**
IEEE Transactions on Smart Grid

REFEREED CONFERENCE PUBLICATIONS

Consumer in-the-Loop: Consumers as Part of Residential Smart Energy Systems **June 2014**
IEEE International Conference on Smart Grid Communications

TECHNICAL REPORT

Monitoring and Feedback System for Improved Building End-Use Efficiency **2013**
EISG Final Report

AWARDS

DOE Apps for Energy Challenge
2012 Grand Prize Student Award

ABSTRACT OF THE DISSERTATION

Residential Demand Response: Generation, Storage, and Load Management

By

Nadia Ahmed

Doctor of Philosophy in Electrical Engineering and Computer Science

University of California, Irvine, 2017

Professor Marco Levorato, Chair

An Energy Management System (EMS) control framework driven by resident behavior patterns is developed. Using hidden Markov modeling techniques, the EMS detects consumer behavior from real-time aggregate consumption and a pre-built dictionary of reference models. These models capture variations in consumer habits as a function of daily living activity sequence. Following a training period, the system identifies the best fit model which is used to estimate the current state of the resident. When a request to activate a time-shiftable appliance is made, the control agent compares grid signals, user convenience constraints, and the current consumer state estimate to predict the likelihood that the future aggregate load exceeds a consumption threshold during the operating cycle of the requested device. Based on the outcome, the control agent initiates or defers the activation request. Using three consumer reference models, a case study assessing EMS performance with respect to model detection, state estimation, and control as a function of consumer comfort and grid-informed consumption constraints is presented. A tradeoff analysis between comfort, consumption threshold, and appliance activation delay is demonstrated.

The EMS system is then extended to include the residential distributed energy management system (DER). In this cyber-physical system, the consumer home generates

and stores energy for utilization by the load to decrease peaks in demand on the power grid. Using historical irradiance datasets a solar irradiance model based on weather forecast data is built to predict the potential future harvested energy of the system in addition to the load profile. The harvested energy and the load are used to assess the amount of energy that may be stored in the energy storage unit of a household. Based on the cost associated with the power rate and the degradation of the battery during the charge discharge cycle, a control policy based on a Markov decision process framework is assessed. A case study for Boulder, CO is presented. Results using the rain flow counting method illustrate a significant reduction in material damage to the battery bank.

Chapter 1

Introduction

The traditional grid maintains a delicate balance between supply and demand. The generation and distribution of electricity from the current power system supplies the absorbing active and reactive load demand. To ensure a reliable "smart" grid, the supply-demand balance must be adaptable to renewables, electric storage, electric transportation, and traditional demand (1).

While most controls are inherent to the electronic circuitry at the generation and distribution stage (i.e. frequency control generators and power converters), fluctuations in load demands must be offset with intermittent generation to avoid grid overload and potential sags. While energy storage solutions such as super capacitors and vanadium redox batteries have been proposed to counteract load noise (2), expense in terms of physical and infrastructural cost render energy storage solutions infeasible compared to traditional generation (3).

Integration of renewables to the traditional grid increases variability and decreases controllability of load balances, as renewables are susceptible to transient availability based on environmental factors. Despite this, the Senate Bill 1078 established the

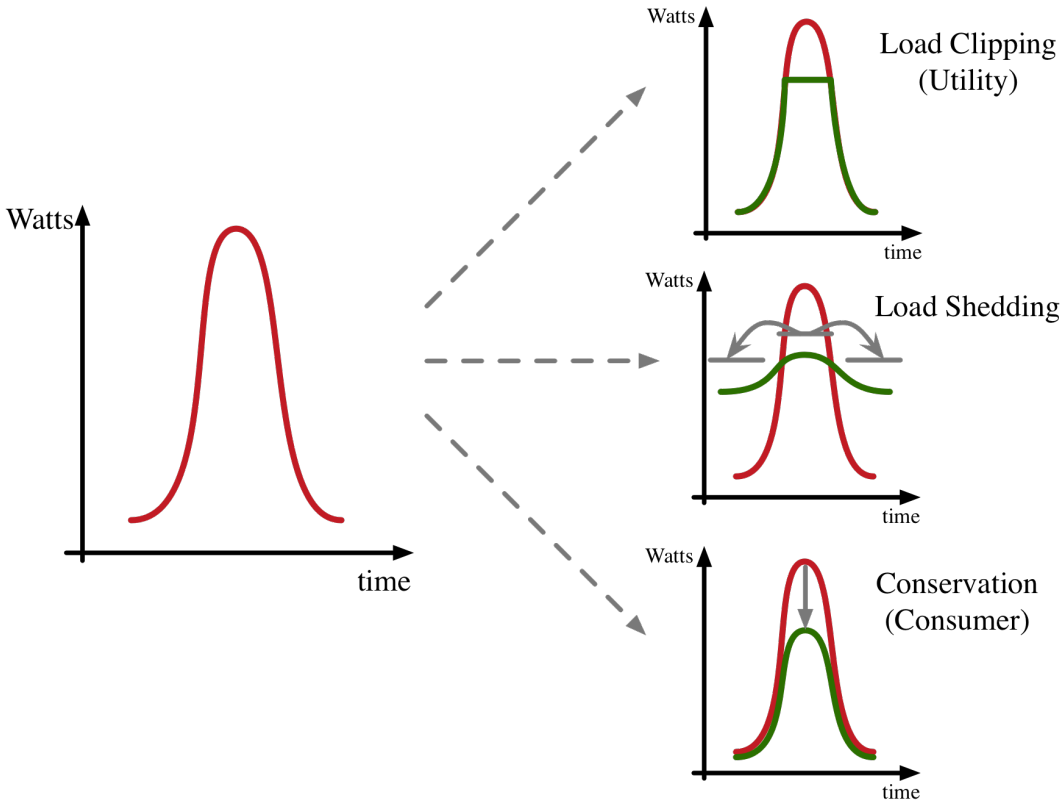

Figure 1.1: Typical Demand Response Schemes.

Renewables Portfolio Standard program requiring 20% renewable energy by 2017 (4). Furthermore, California's RPS program seeks to increase energy acquisition from renewables to 33% by 2020 (5). The push for successful renewable integration complicates traditional power system performance by introducing noise to the line. As is, the power grid is susceptible to control error due to noise on the order of +/- 100MW. By integrating 20% more distributed renewable energy sources control errors increase several times the existing error. 33% integration, as encouraged by California's RPS, would result in over +/-3000MW of control errors to the existing grid(6). With the shift to 33% renewables, existing grid infrastructure would set off protective devices, thereby interrupting power flow to residents and resulting in blackouts. Demand Response [DR], however, is an immediate, cost-effective, and significant improvement to grid balancing and smoothing of transients. "...DR can directly reduce CO_2 emissions by 1 percent...[which is equivalent to]...19.5 million metric tons (7)."

1.0.1 Current Demand Response Programs

Instead of increasing supply, demand response programs seek to decrease peaks in consumer load by promoting energy efficiency and conservation through monetary incentives. These programs require involuntary or voluntary participation of consumers. Involuntary programs via Automated Demand Response (AutoDR) systems give direct control to the utility enabling it to clip peaks in load during periods of high demand. In the industrial and commercial context alone, fast Automated Demand Response systems could double load shedding potential between .42 and 2.07 GW, successfully counteracting variability in grid balance caused by intermittent renewables (8). However, 22% of US total energy consumption is from the residential sector (9) representing the greatest "untapped" potential for demand response programs (10).

Current residential AutoDR systems are promoted for discretionary loads associated with heating and cooling in exchange for rebates. In contrast to industrial and commercial sectors, the popularity of such systems are low as residential consumers are unlikely to give up autonomy of their homes to the utility. Voluntary programs using Advanced Metering Infrastructure (AMI) rely on consumer compliance to grid alerts and pricing strategies to shift loads to off-peak hours thereby flattening demand. Time of use (TOU) pricing sets electric prices according to time of day while dynamic pricing relies on real-time power system conditions based on metering data. When provided with AMI dynamic pricing programs, though representing only 17% of demand response potential, residents have the impact to provide 45% peak reduction (10). The goal of these demand side programs is to use financial incentives provided by the utility to influence consumption patterns indirectly thereby achieving a manageable load profile.

Demand response programs would benefit significantly from residential sector penetration. This sector alone consumes 22% of US total energy (9) and is growing rapidly. From 1980-2009, residential electricity consumption increased by 57.2% due to housing and population growth alone (11). For programs representing 17% of demand response potential, residential participation has the impact to provide a 45% reduction in peak loads (10).

1.0.2 Energy Management Systems

However, only 10% of residents enroll in demand response programs and even fewer are compliant (12). These programs require involuntary or voluntary participation of consumers in exchange for utility-provided monetary incentives. Involuntary automated demand response (AutoDR) gives direct control to the utility enabling it to

clip peaks in demand for discretionary loads associated with heating and cooling in exchange for rebates. However, the acceptance of such systems are low as residential consumers are unlikely to give up autonomy of their homes to the utility. In contrast, voluntary programs using Advanced Metering Infrastructure (AMI) rely on consumer compliance to grid alerts and pricing strategies to manually shift loads to off-peak hours preserving resident autonomy at the expense of convenience. For example, to make informed appliance scheduling decisions, the user must examine their energy bill, understand their aggregate power consumption, maintain an active knowledge of contributing appliances, and be aware of outside grid conditions. Utility pricing strategies such as time of use (TOU) pricing, dynamic pricing (DP), and critical peak pricing (CPP), further complicates user load shifting decision-making.

Energy Management Systems (EMS) offer a partial solution to obstacles in current residential demand response programs. These systems utilize the convenience of automated demand response without compromising residential autonomy. Such systems, validated through simulated case studies, assume pricing as a driving factor for residential consumption behavior and measure consumer satisfaction indirectly through utility function parameters (13; 14; 15; 16). In other words, EMS methods are constructed from various cost-benefit analyses to shift loads to times corresponding to minimal cost. If successfully integrated to the residential sector, price driven energy management would shift many consumer loads to off-peak times. Thus, instead of flattening the residential sector consumption peak, scheduling could potentially result in a shift in the original peak with respect to time. In this scenario, load peaks would remain unchanged and utility pricing schemes would be adjusted to take into account popular demand.

The effectiveness of price-driven energy management frameworks would benefit by including consumer behavior as a variable in the optimization of "shiftable" appli-

ance scheduling. Pricing as a reward for energy curtailment has shown to wear off with time in other behavioral domains. Furthermore, the sustainability of monetary incentives is unclear for the long term, which could potentially result in a rebound in demand behavior exceeding pre-program levels should these incentives no longer be provided (12). It becomes necessary to examine the source of demand–the individual consumer. Residential consumer behavior must be examined to predict habitual consumption patterns, improve existing EMS scheduling algorithms, and provide user feedback with respect to consumption as a function of behavior.

Inclusion of the consumer as part of EMS framework presents challenges due to the nonlinearity and complexity of human behavior. To address this we take a specific human behavior modeling approach to build a system that directly includes the resident in the system feedback loop to drive the scheduling of appliances. Similar to proposed EMS, the improved EMS shift loads, but does so dynamically–providing the individual consumer with a unique real-time load control mechanism as a function of behavior. In contrast to offline data driven activity pattern discovery, this method requires prebuilt models facilitating dynamic recognition of daily activity sequences sufficient for the appliance scheduling control.

In this paper we make the following contributions to existing energy management system frameworks:

- Given a household appliance inventory, we build a dictionary of reference models for a single residence as a means of detecting structured general behavioral activity from real-time AMI aggregate consumption observations.
- We dynamically detect resident behavior sequences and patterns from AMI aggregate consumption during a training period whereby the best fit reference model is identified. Following training, the EMS can estimate the current be-

havioral states as a function of the current consumption.

- For an appliance activation request, we implement appliance scheduling using an activity informed "on-off" control mechanism. The EMS interfaces with AMI to receive real-time DR consumption constraints, predicts the likelihood of exceeding these constraints based on the current user state, best fit model, requested appliance, user convenience, and current electric load.

- We perform a case study instantiating the improved EMS to schedule a continuous cycle deferrable appliance load and assess the performance in terms of appliance activation delay and user comfort.

1.1 Distributed Resources and Storage

We would also like to approach the study by including work towards a more unified model by including distributed energy resources such as photovoltaic cells that the residence may install in their home to comply to government renewable programs. In this two-pronged study, while the first study explores the relationship of individual human behavior, the second study examines the interaction of the resulting load curve with the irradiance as well as with battery storage. Battery storage is becoming a more available option a manufacturer's are outputting a wider variety of battery's for use in the home. Most notable is the Tesla Powerwall which is a lithium ion battery directly interfacing with solar cells. In this problem we consider the entire residential system in terms of the load, irradiance, and battery components to derive the best control algorithm to minimize battery degradation and decrease overall grid cost. We are particularly attentive to expressing the irradiance available to the household based on predicted weather forecasts as a means of inferring the future irradiance states in order to better plan the charging and discharging of the battery or to take power from

the grid. While (17) offered a similar model that included the irradiance, they did not take into account the weather forecast or the cloud cover in the calculations. Instead, they directly calculated the ground level irradiance conditions by using atmospheric relations, geographic location, solar tilt angle, earth's tilt angle, and various physical parameters using publicly available datasets. While they studied the irradiance, they did not include the battery as a part of the home generation, storage, and distribution center. In related work, (18) explored the battery in communications applications for energy harvesting. In this work the examined the degradation that the battery faced depending on a variety of factors and sought to control the state of charge of the battery. (19) introduced a more holistic approach to solar-powered embedded systems that took into account the state of charge of a battery as well as the weather in a simplified model. We would like to extend the research presented in (19) by including a more complex model based on data gathered from weather news outlets in terms of forecast for a specific region in the United States, as well as data provided by NREL, a laboratory that studies variations in irradiance in the same region. We would like to therefore, based on cloud cover, irradiance, and load data build a Markov based model which we implement control to:

- Control battery degradation over time
- Minimize the electric cost to the resident

By combining both approaches, consumer-centric demand response with demand response in terms of residential generation and storage as well, we may derive a unified approach to residential microgrids and offer users greater control over their energy usage as well as decisions concerning energy generation.

Chapter 2

Methods

2.1 Discrete Time Markov Chains

In this section we introduce the basic properties and characteristics of Markov chain to provide a foundation to extensions with respect to this fairly simple mathematical model. By understanding the concepts of a Markov chain, one can fully appreciate the optimization framework used in the residential demand response system proposed in this study. After identifying key concepts in Markov chains, mathematical extensions such as hidden Markov models and Markov decision processes will be presented as methods for the EMS agent to learn from sensory data. We choose to use a Markov construction of system parameters as they are used extensively in applications central to human behavior as well as the fact that Markov property allows for a simple recursive or iterative means for solving nonlinear problems. To begin our study we delve into Markov chains. At a base level, a Markov chain can be described as a stochastic process where present is all the information about the past that is relevant for predicting the future (20).

2.1.1 A Markov Chain as a Filtration

A Markov chain is what is known as a natural filtration. Let $(\mathcal{F}_n, n \in \mathbb{Z})$ represent a sequence of σ fields on the path space Ω with $\mathcal{F}_n \subseteq \mathcal{F}_{n+1}$ for all $n \geq 0$. A filtration represents an increasing stream of information, more specifically $\mathcal{F}_n$ form an increasing family of algebras. In the case of $\mathcal{F}_n$ this is the information provided by the first n variables. A stochastic discrete-time process $X = (X_n, n \in \mathbb{Z})$, is adapted to the filtration generated by X, $\mathcal{F}_n$ if:

$$\sigma(X_n) \subseteq \mathcal{F}_n \ \forall n \ \geq 0 \tag{2.1}$$

In other words, given a random variable $X(n)$, $\mathcal{F}_n$ represents all information known about X up until the time n. In discrete time, X can be expressed as the information $X(0), \ldots, X(n)$. For $\mathcal{F}_{n+1}$, we notice that X corresponds to the information $X(0), \ldots, X(n), X(n+1)$. $\mathcal{F}_n$ is indeed a subset of $\mathcal{F}_{n+1}$ as we recognize that the first t terms in $X(n+1)$ are also members of $X(n)$. The discrete path space Ω represents the set of all possible outcomes of a probability experiment. For X the generalized path space can be described as $x_{[1:T]} = (x_1, x_2, \ldots, x_T),\ x_n \in \mathcal{S}$. We summarize the general probabilistic quantities in Table 2.1.

n	discrete time
$\mathcal{S}$	state space of $X(n)$
Ω	path space $X(0), X(1), \ldots, X(T)$
$\mathcal{F}_n$	information/filtration until n

Table 2.1: Markov chain parameters

2.1.2 The Markov Property

Let Ω represent the path space of the discrete time stochastic process X. $P(\bullet)$ is a distribution on Ω describing the dynamics of X. $P(\bullet)$ has the Markov property if for all $x \in \mathcal{S}$ and $n = 1, \ldots, T-1$

$$P(X_{n+1} = x_{n+1} | \mathcal{F}_n) \tag{2.2}$$

$$P(X_{n+1} = x_{n+1} | X_1 = x_1, \ldots, X_n = x_n) \tag{2.3}$$

$$= P(X_{n+1} = x_{n+1} | X_n = x_n) \tag{2.4}$$

Presenting an alternative notation, the probability of a x to y transition in one step starting at time n for a stochastic process X given the distribution $P(\bullet)$ may be expressed as:

$$p_{n,xy} = P(X_{n+1} = y | X_n = x) \tag{2.5}$$

$$= P(x \to y) \tag{2.6}$$

Examining the probability of an additional step into the future, or the transition from $x \to y \to z$ starting from time n for a stochastic process X with distribution $P(\bullet)$ is:

$$P(X_{n+2} = z \cap X_{n+1} = y | X_n = x) \tag{2.7}$$

Which we can rewrite using Baye's Rule to:

$$P(X_{n+2} = z | X_{n+1} = y \cap X_n = x) P(X_{n+1} = y | Xn = x) \tag{2.8}$$

and simplify to

$$= P(X_{n+2} = z|Xn + 1 = y)P(X_{n+1} = y|X_n = x) \tag{2.9}$$

$$= p_{n+1,yz} \cdot p_{n,xy} \tag{2.10}$$

using the Markov property which applies to the entire future path of X irrespective of the number of steps from n into the future. We take advantage of the Markov property when calculating the path probabilities starting with the initial state probability which is expressed as:

$$\pi_0(x_j) = P(X(0){=}x_j) \tag{2.11}$$

We can then write the path probabilities in terms of the initial probability for the general case as:

$$P(X(0){=}x(0), \ldots, X(T){=}x(T)) = \pi_0(x(0)) \prod_{n=0}^{(T-1)} P_{x(n),x(n+1)} \tag{2.12}$$

The Markov chain is said to be *homogeneous* in time or *stationary* if the transition probabilities of X expressed by the distribution $P(\bullet)$ is independent of n. In the above example, this would reduce the expression

$$P(X_{n+2}{=}z|Xn + 1{=}y)P(X_{n+1}{=}y|X_n{=}x) = p_{n+1,yz} \cdot p_{n,xy}, \quad \text{to}$$

$$= p_{yz} \cdot p_{xy}. \tag{2.13}$$

2.1.3 The Forward Equation

We can thereby repackage the information learned thus far with respect to Markov chains by deriving an expression describing how the probabilities of transitions evolve

over time in the form of what is known as the *forward equation* more popularly known as the Chapman-Kolmogorov equation (21). This expression provides a great deal of insight with respect to the visible simple Markov chain where $X(t)$ is observable for all discrete time up to n. We later extend the forward equation for the hidden Markov chain. Let p_{yx} represent the transition probabilities of a discrete state space Markov chain. We write

$$u_n(y) = P(X_n = y) \tag{2.14}$$

The forward equation (aka Chapman-Kolmogorov) is a formula for u_{n+1} in terms of u_n

$$\begin{aligned} u_{n+1}(x) &= P(X_{n+1} = x) && (2.15)\\ &= \sum_{y\in\mathcal{S}} P(X_{n+1} = x \cap X_n = y) && (2.16)\\ &= \sum_{y\in\mathcal{S}} P(X_{n+1} = x | X_n = y) \cdot P(X_n = y) && (2.17)\\ &= \sum_{y\in\mathcal{S}} P(X_n = y) \cdot P(X_{n+1} = x | X_n = y) && (2.18)\\ &= \sum_{y\in\mathcal{S}} u_n(y) p_{yx} && (2.19) \end{aligned}$$

Forward Equations in Matrix Form

Suppose that the state space is finite and $\mathcal{S} = \{x_1, \ldots, x_m\}$. We rewrite state j to imply the state x_j. In other words, we express, $u_{n,j} = P(X_n = x_j)$ as $u_{n,j} = P(X_n = j)$. We can collect the probabilities into $1 \times m$ row vector $\mathbf{u_n} = (u_{n,1}, \ldots, u_{n,m})$.

The transition matrix $\mathbf{P}$ is the $m \times m$ matrix of transition probabilities (i, j), where the entry of $\mathbf{P}$ is $p_{ij} = P(i \to j) = P(X_{n+1} = j | X_n = i)$ and for each row k,

$\sum_{n=1}^{m} p_{kn} = 1$. We may express the forward equations in matrix form recursively. For example,

$$\mathbf{u_{n+2}} = \mathbf{u_{n+1}P} = (\mathbf{u_n} \cdot \mathbf{P}) \cdot \mathbf{P} = \mathbf{u_n P}^2,$$

for a distribution that is (stationary) homogeneous with respect to time. We thereby generalize the Chapman-Kolmogorov forward equations using the following matrix notation:

$$u_{n+1,j} = \sum_{i=1}^{n} u_{n,i} P_{ij} \tag{2.20}$$

$$\mathbf{u_{n+1}} = \mathbf{u_n P} \tag{2.21}$$

By expressing the forward equations in this manner allows us to study the evolution of the Markov chain probability using eigenvalues and eigenvectors.

2.2 Hidden Markov Models

The basic principles of Markov chains discussed thus far are in the context of a fully observable or visible sequence of states whose path probability can be calculated readily. However, there may be variables that influence the evolution of the chain but are not directly observable. These hidden variables may be observed indirectly by observing the chain for a period of time long enough to identify them to be able to change future state predictions (20). Taking this even further, the Markov chain itself may not be observable. In other words, how can we reason about a series of states in a Markov chain if we cannot observe the states themselves but rather only some probabilistic function of those states? The hidden Markov model (HMM) presents a

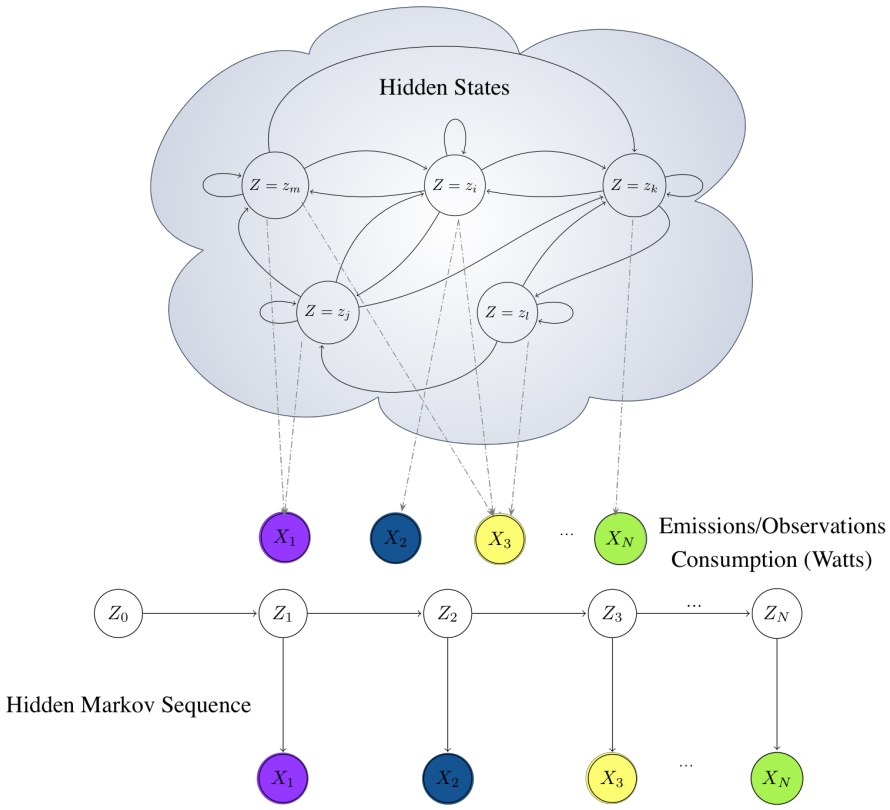

Figure 2.1: Description of the hidden Markov model (HMM) adapted from (23).

case where observations are a probabilistic function of Markov chain state–a doubly embedded stochastic process (22). In other words we can only observe the hidden discrete states of the Markov chain through another set of stochastic processes that produce a sequence of observations driven from the chain of interest. HMMs are particularly interesting because they can deal with nonlinear system evolution and measurements. Furthermore, the HMM can only be in one state at a time thereby limiting the representational capacity of the modeled system.

2.2.1 HMM description

We describe the HMM in terms the following terms:

- n represents discrete time with N being the final time trial.
- $\mathcal{N}$ is the number of states in the state space of the hidden Markov process.
- $Z(n)$ is the random variable describing the hidden Markov process such that $Z(n) = \{Z_1, \ldots, Z_{\mathcal{N}}\}$ is drawn from the state alphabet.
- M is the number of possible observations per state.
- $X(n)$ is the random variable describing observations or emissions of the state variable $Z(n)$. $X_n = \{x_1, \ldots, x_M\}$ Observations at time n do not depend on the previous states or observations given the states. Therefore, observations emitted by the hidden Markov chain are independent of past observations. The output independence assumption is as follows:

$$P(X(n)=x_k|X(1)=x_1,\ldots,X(N)=x_n, Z(1)=z_1,\ldots,Z(n)=z_j) = P(X(n)=x_k|Z(n)=x_j) \tag{2.22}$$

- $P_{ij} = P(Z(n+1) = z_j|Z(n) = z_i),$ for $1 \leq i, j \leq \mathcal{N}$ is the transition matrix for the hidden Markov chain which is unobservable.
- $B_{jk} = P(X(n) = x_k|Z(n) = z_j),$ for $1 \leq i \leq \mathcal{N}, 1 \leq k \leq M$ is the probability of the hidden state z_j generating the observation x_k. As implied B_{jk} is a matrix of dimension $\mathcal{N} \times M$.
- $\pi_i = P(Z(1) = z_i)$, where $1 \leq i \leq \mathcal{N}$ describes the initial distribution of the hidden Markov chain.

2.2.2 HMM Forward Probabilities

We would like to take the forward equations for the fully observable Markov chain and adapt it for the HMM case. To do this we are given the observation sequence:

$$X(1) = x_1, X(2) = x_2, \ldots, X(N) = x_N \quad \text{or shortening the notation}$$
$$X_1 = x_1, X_2 = x_2, \ldots, X_N = x_N$$

From this observation sequence we would like to calculate:

$$\alpha_i(N) = P(X_1 = x_1, X_2 = x_2, \ldots, X_n = x_n, \ldots, X_N = x_N, Z_N = z_i) \tag{2.23}$$

for a model with parameters $\lambda = (\pi_i, P_{ij}, B_{jk})$ as introduced. We follow the same method for the calculation of the forward variables as in the visible Markov chain case. We simply calculate the path probabilities starting at the initial distribution and continuing to the next time step until we establish a general relationship. At the initial time step which we will establish as $n = 1$ (though some sources may label the first step as $n = 0$) we find:

$$\alpha_i(1) = P(Z_1 = z_i, X_1 = x_j) = P(X_1 = x_j | Z_1 = z_i) \cdot \Pi(z_i)$$

or in matrix form:

$$\alpha = \mathbf{\Pi^{\intercal} B}$$

For the next time step we find the forward path probabilities as follows:

$$\begin{aligned}
\alpha_k(2) &= P(Z_2 = z_k, X_2 = x_l, X_1 = x_j) \\
&= \sum_{q=1}^{\mathcal{N}} P(Z_2 = z_k, X_2 = x_l, Z_1 = z_q, X_1 = x_j) \\
&= \sum_{q=1}^{\mathcal{N}} P(X_2 = x_l | Z_2 = z_k, Z_1 = z_q, X_1 = x_j) P(Z_2 = z_k, Z_1 = z_q, X_1 = x_j) \\
&= \sum_{q=1}^{\mathcal{N}} P(X_2 = x_l | Z_2 = z_k) P(Z_2 = z_k | Z_1 = z_q, X_1 = x_j) P(Z_1 = z_q, X_1 = x_j) \\
&= \sum_{q=1}^{\mathcal{N}} P(X_2 = x_l | Z_2 = z_k) P(Z_2 = z_k | Z_1 = z_q, X_1 = x_j) \alpha_q(1) \\
&= \sum_{q=1}^{\mathcal{N}} \alpha_q(1) P(X_2 = x_l | Z_2 = z_k) P(Z_2 = z_k | Z_1 = z_q)
\end{aligned}$$

We may generalize this equation to:

$$\alpha_k(n+1) = \sum_{q=1}^{\mathcal{N}} \alpha_q(n) P(X_{n+1} = x_l | Z_{n+1} = z_k) P(Z_{n+1} = z_k | Z_n = z_q) \tag{2.24}$$

or in matrix form:

$$\alpha_{\mathbf{n+1}} = \alpha_{\mathbf{n}} \cdot \mathbf{P} \cdot (\mathbf{B}_{\mathbf{X_{n+1}=x}} \mathbb{I}) \tag{2.25}$$

where $\mathbb{I}$ represents the identity matrix.

2.2.3 Model Detection

From the forward probability we can calculate the likelihood of a variety of HMMs with differing parameters $\lambda = (\pi_i, P_{ij}, B_{jk})$ for a specific observation sequence using

the maximum likelihood estimate. Since the number will be small for each time step evaluated, this value can be scaled by the maximum forward probability calculated. In other words the HMM construction allows the agent to detect and classify observations to a particular reference model λ_i defined by $(\Pi_Z^{(i)}, P(Z_{n+1}^{(i)}|Z_n^{(i)}), P(X_n|Z_n^{(i)}))$ for $1 \leq i \leq \max(\mathcal{S}_{\lambda_i})$ from a dictionary of models within a training period T. Following the training period T, the identified model λ_i is used to calculate the maximum likely hidden state Z_n which allows the system to predict the likelihood of future observations X_n for a rolling time horizon. The resulting observation predictions inform real-time decisions with respect to the type of control we seek to optimize. In order to calculate the best fit reference model, λ_i for an observation sequence we utilize the forward algorithm for HMMs to calculate the posteriori probability during the training period T.

2.2.4 Model Detection

Given the observation sequence: $X_1{=}x_j, \ldots, X_T{=}x_z$, we may calculate:

$$\alpha_k(s){=}P(X_1{=}x_j, \ldots, X_T{=}x_z, Z_k{=}s)$$

for a specific model λ_i defined by $(\Pi_Z^{(i)}, P(Z_{t+1}^{(i)}|Z_t^{(i)}), P(X_t|Z_t^{(i)}))$ or in matrix format: $(\mathbf{\Pi}_{\lambda_i}, \mathbf{P}_{\lambda_i}, \mathbf{B}_{\lambda_i})$. For the first time step we calculate the probability of the joint distribution of the first hidden state and observation using the initial distribution of the hidden chain. $\alpha_1^{(i)}(s){=}P(X_1{=}x_j, Z_1^{(i)}{=}s) = \Pi_{Z_1}^{(i)}(s)P(X_1{=}x_j|Z_1^{(i)}{=}s)$, or

$$\alpha_1^{(i)}{=}\mathbf{\Pi}_{\lambda_i}^{\top} \cdot \mathbf{P}_{\lambda_i}. \tag{2.26}$$

We may generalize the remaining forward calculations for $1 \leq t \leq T-1$ as

$$\alpha_{t+1}^{(i)} = \alpha_t^{(i)} \cdot (diag(\mathbf{B}_{X_{t+1=x}})_{\lambda_i}) \cdot \mathbf{P}_{\lambda_i}. \tag{2.27}$$

To classify the sequence according to a particular model we evaluate

$$\sum_{r \in \mathcal{S}_{Z^{\lambda_i}}} \alpha_T^{(i)}(r), \tag{2.28}$$

where T is the training period. The model λ_i that results in the maximal value is then identified as the approximate reference class for the real-time observations sensed by the system.

2.2.5 State Estimation based on Model

Once a reference class for a sequence of training observations $X_1 = x_j, \ldots, X_T = x_z$, is determined ($\lambda_i = \lambda$), the state estimate may be calculated by propagating the forward a posteriori probability value for the new real-time consumption observations using the statistics, $(\mathbf{\Pi}_\lambda, \mathbf{P}_\lambda, \mathbf{B}_\lambda)$, of the reference class. Since we have identified the best fit model according to the visible observations, we drop the λ_i in our notation in this section to increase readability. We can scale the forward joint probability value to obtain a distribution of states. In other words, given the sequence $X_{T+1} = x_a \ldots, X_t = x_b$ we are interested in calculating

$$P(Z_t = s | X_{T+1} = x_a, \ldots, X_t = x_b) = \frac{\alpha_t(s)}{\sum_{r \in \mathcal{S}_Z} \alpha_t(r)}. \tag{2.29}$$

The state $Z_t = s$ that results in the greatest probability given the observation sequence is defined as the maximum likelihood estimate.

2.2.6 Stochastic Control: Taboo States

We can thereby partition the state space of Z_t into two sets, the "taboo" set, H_Z corresponding to $X_t = C_t + E_t + F_t \geq z - d_t$, and its complement H_Z^{c}. We then rearrange the states of $P(Z_{t+1}|Z_t)$ to the following format:

$$P(Z_{t+1}|Z_t) = \begin{bmatrix} \mathbf{T_Z}(\mathbf{1},\mathbf{1}) & \mathbf{T_Z}(\mathbf{1},\mathbf{2}) \\ \mathbf{T_Z}(\mathbf{2},\mathbf{1}) & \mathbf{T_Z}(\mathbf{2},\mathbf{2}) \end{bmatrix} \tag{2.30}$$

where $\mathbf{T_Z}(\mathbf{1},\mathbf{1})$ represents the sub-matrix of states which transition from $H_Z^{\mathsf{c}} \rightarrow H_Z^{\mathsf{c}}$, $\mathbf{T_Z}(\mathbf{1},\mathbf{2})$ represents the sub-matrix of states which transition from $H_Z \rightarrow H_Z^{\mathsf{c}}$, $\mathbf{T_Z}(\mathbf{2},\mathbf{1})$ represents the sub-matrix of states which transition from $H_Z^{\mathsf{c}} \rightarrow H$, and $\mathbf{T_Z}(\mathbf{2},\mathbf{2})$ represents the sub-matrix of states which transition from $H_Z \rightarrow H_Z$ (24).

The total probability of transitioning from H_Z^{c} to the set H_Z within a finite time horizon, N, defined by the operational cycle of d_t, can be calculated using the sub-matrices of the rearranged transition matrix as

$$P_{\mathbf{T_Z}(\mathbf{1},\mathbf{2})}(N) = \sum_{s \in \mathcal{S}_H} \sum_{n=1}^{N} \mathbf{T_Z}(\mathbf{1},\mathbf{1})^{n-1} * \mathbf{T_Z}(\mathbf{1},\mathbf{2}). \tag{2.31}$$

This probability provides the system agent a means of predicting the observation sequences for a finite time horizon, N, as well as a probability measure as with respect to a constraint.

2.3 Markov Decision Process

A Markov decision process (MDP) is essentially a Markov chain whose state at any given time is used to determine an action. Associated with this state-action is a particular income viewed either a cost or reward for executing a particular action upon a state. The action influences the transition of the system state to the next state of the Markov chain. We describe the sequence of actions taken upon states as a policy. More specifically a policy is deemed optimal if it optimizes the expected cumulative value (total income accrued) either through the minimization of cost or the maximization of reward. The process can be evaluated through different techniques such as constrained linear optimization, policy iteration, or value iteration algorithms. The focus of this work utilizes the value iteration algorithm specifically.

As introduced in (25) we consider a system with a finite discrete state space $s \in \{s_1, s_2, \ldots, s_S\}$, where S represents the number of states. At a specific time instant $n \in \mathbb{N}^+$ we may observe the current system state s_i and select an action a_k from a finite set of states $a \in \{a_1, a_2, \ldots, a_A\}$ where A represents the finite number of actions. Upon selecting an action $A_n = a_k$ on the current state $S_n = s_i$ the system receives an reward $R(S_n = s_i, A_n = a_k)$ which we would like to maximize. Alternatively, the reward may be expressed as a cost $C(S_n = s_i, A_n = a_k)$ over which we would like to minimize.The system then moves to the next state $S_{n+1} = s_j$ with probability $P(S_{n+1}{=}s_j | S_n{=}s_i, A_n{=}a_k)$.

A discount factor γ, $0 \leq \gamma \leq 1$ determines the value of unit income $\ltimes$ time steps in the future as $\gamma^{\ltimes}$.

The goal with this framework is to select a policy π, or a sequence of state-actions $< S_1, A_1 >, < S_2, A_2 >, \ldots$ to maximize the cumulative reward accrued or minimize the cumulative cost.

The quality of a policy is gauged by the value function which associates to each state the expected cumulative discounted reward from starting in a considered state and following a given policy. An optimal policy maximizes the associated value for each state. If the model is known and state and action spaces are small enough, the optimal policy can be computed using dynamic programming or value iteration. In value iteration we compute directly the optimal value function using nonlinear Bellman optimality equations and an iterative scheme which takes advantage of the Markov property discussed thus far.

2.3.1 Stochastic Control: An Optimal Policy

To calculate an optimal policy for the system given the current observed state of the Markov process we may use policy iteration, linear programming, or value iteration techniques. In policy iteration we evaluate an initial policy and compute its associated value using the linear Bellman evaluation. We associate to each state the action which maximizes expected cumulative reward obtained from starting in a particular state, applying an action and following the initial policy. We evaluate and improve the policy, recalculate the policy, and stop iteration until convergence is reached in a finite amount of steps. In value iteration we compute directly the optimal value function using nonlinear Bellman optimality equation and an iterative scheme based on the fact that the value function is the unique fixed point of the associated Bellman operator. An optimal policy is greedy with respect to value function. Linear programming sets up the system as a constrained convex optimization problem which can be solved using a system of linear equations. In value iteration, the technique used in this study, we compute directly the optimal value function using nonlinear Bellman optimality equation and an iterative scheme based on the fact that the value function is the unique fixed point of the associated Bellman operator (26). An optimal policy is

greedy with respect to value function.

To summarize, given the states S, the model $P(Sn+1 = s'|S_n{=}s, An{=}a)$, the actions $A(S_n)$, the reward/cost $R(S_n{=}s)$, $R(S_n{=}s, A_n{=}a)$, $R(S_n{=}s, A_n{=}, Sn+1{=}s')$ may be be defined on the state, the state-action selected, or the transition. The policy $\pi(S_n) \rightarrow A_n{=}a$ can be described as the sequence of state action pairs in the form $< s, a >, < s, a >, \ldots$ while an optimal policy π^* is defined based on the optimal reward/cost maximization/minimization $< s, a, r >, < s', a', r' >, \ldots$ across all possible state-action pairs for the current state. The Bellman equations are:

$$V(s) = \max_a (R(s,a) + \gamma \sum_{s'} P(s'|s,a)V(s')) \tag{2.32}$$

$$Q(s,a) = R(s,a) + \gamma \sum_{s'} P(s'|s,a) \max_a Q(s',a') \tag{2.33}$$

We typically use the Q-state form of the Bellman equation for reinforcement learning espectially when the reward or transition functions are not known in advance. Figure 2.2 illustrates the value function iteration technique for a state space containing three values $S_n = \{s_1, s_2, s_3\}$ represented by the triangles. The tree starts its way from the bottom at the calculation of V_0 for each state. In the example each state may choose from two actions $A_n = \{a_1, a_2\}$. The Q-states are represented by the circles for each possible action. To calculate the Q-state the Bellman equation of the second form is used. The value at the next iteration or time step is determined by taking the action and assigning the value of the winning Q-state to the V_1.

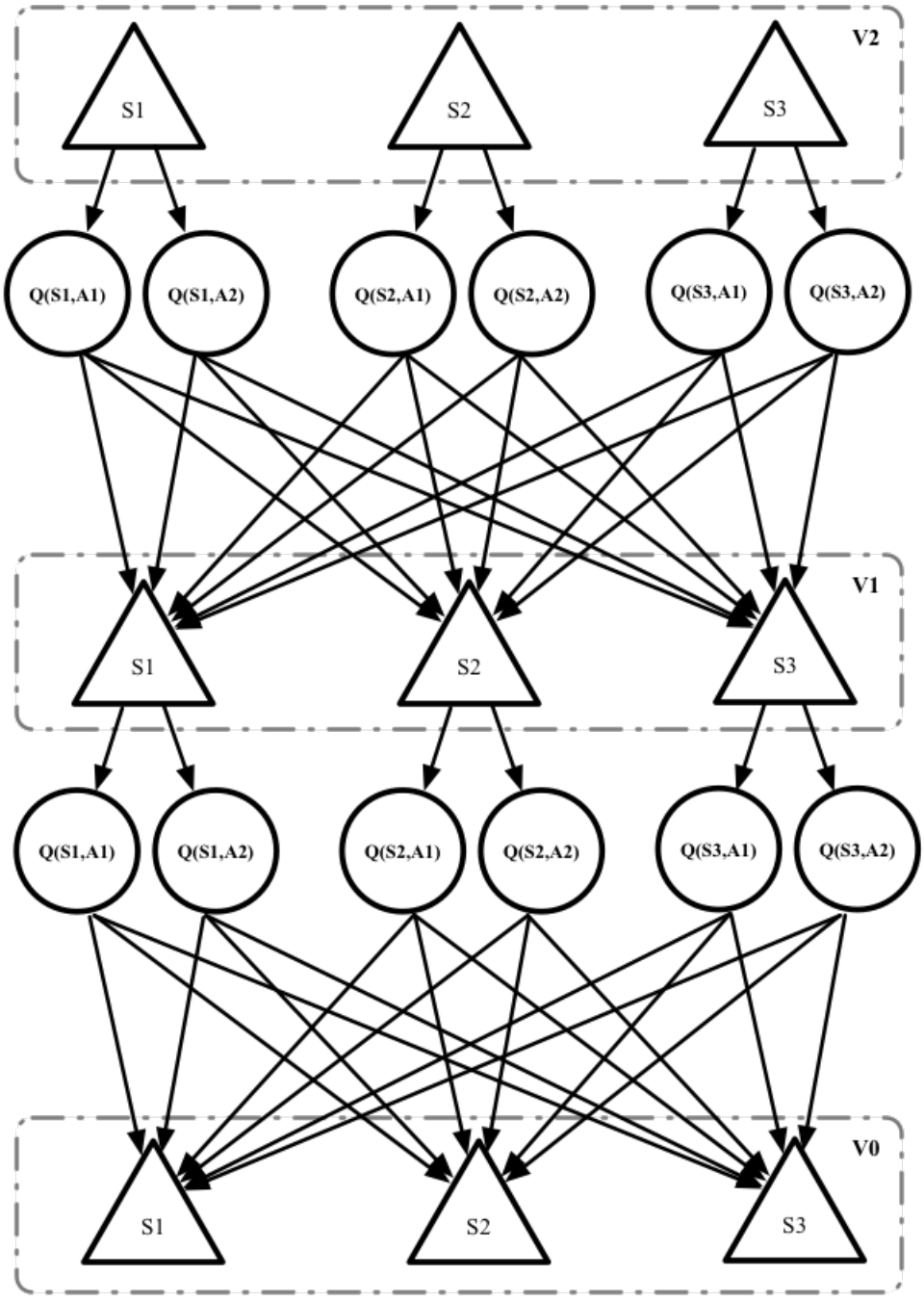

Figure 2.2: Decision tree of the Markov process. The value is determined by optimizing over the sum of the expected reward/cost for each Q-state or state-action pair. Typically the maximum reward or conversely minimum cost state-action value is selected at each time step.

Chapter 3

Consumer Centric Demand-Side Management

3.1 Energy Management System (EMS)

The EMS is an intelligent automated control agent that dynamically learns consumer behavior, analyzes and predicts future behavior, and schedules and controls appliances with respect to behavior and grid signals. Central to the system is the resident energy consumer. Their habits and activities of daily life are what drive their consumption profile. It therefore becomes imperative for the intelligent agent to learn typical user behavior based on patterns in load profiles. The system does so by comparing sensed electricity consumption to pre-built general consumer models and prior information with respect to the inventory of appliances in the home. Following a training period and successful dynamic model detection, the agent continues to receive consumption information allowing the system to estimate current and future resident states based on the model. However, decoding consumer activity alone is not the objective of

the EMS. The goal of the EMS is to perform appliance scheduling based on current *consumer activity*, *appliance* energy requests, *grid signals*, and user *convenience* parameters. The system thus serves to interface between complex systems in order to make decisions with respect to the activation of cyclic "shiftable" loads to improve residential consumer demand response.

3.1.1 Consumer Activity:

Human behaviors exhibit hierarchical structure according to goals and recursive implementation of sub-goals (27). In the home, activities of daily life drive energy consumption dictating which appliance will be initiated at any given time. Realizing the significance in encoding hierarchy, we propose a modeling framework that captures dependencies between finite human activity units and appliances. In other words, we can simplify residential behavior into sequences of activity states that cannot be directly measured. For example, activity states such as *hygiene*, *cook*, *clean*, or *rest* each have unique effects on consumer load profile as well as which appliances may be activated. Different sequences of activities characterize user schedules and provide a basis for building a dictionary of typical consumer models used by the EMS to detect daily user behavior and make scheduling decisions.

3.1.2 Appliances:

Each consumer activity influences appliance usage. For example, if a user is *cleaning*, they are likely to use appliances such as a vacuum, a washing machine, or a steamer. Given the inventory of household devices, we capture these dependencies by grouping short operating appliances according to their most likely activity. Doing this allows us to compress the state space of these "on-off" appliances by activity. Larger appli-

ances that have longer operating periods are classified as either "shiftable" or "non-shiftable" activity independent or dependent long-term devices. These devices may operate over multiple behavior activities and cannot be compressed in state space. In fact, the EMS seeks to control and schedule "shiftable" larger appliances due to their heavy influence on load profile. We then build a table of all possible combinations of compressed activity-short-term-appliance grouping as well as the uncompressed larger appliance states, allowing us to characterize activity influenced consumption load profiles.

3.1.3 Grid Signaling:

Consumption constraints are taken as an input to the control agent directly from the AMI. These constraints may be consumption restrictions (kWh) placed in the form of an alert or as a function of TOU or dynamic pricing (DP) schemes. The EMS takes into account the constraint when making scheduling decisions.

3.1.4 Consumer Convenience:

The resident may also set a convenience constraint with respect to the activation delay of "shiftable" appliances should the grid constraint be strictly met. Depending on the current activity of the user, deferring loads to a later time based on grid conditions alone may be undesirable. Thus, consumer constraints allow the user to have a degree of freedom with respect to appliance scheduling without having to override the energy management system.

To understand how consumer activity, appliances, grid signaling, and consumer convenience interact in the EMS, one may consider the case where a resident makes an energy request for the activation of a heavy "shiftable" appliance. At the instant

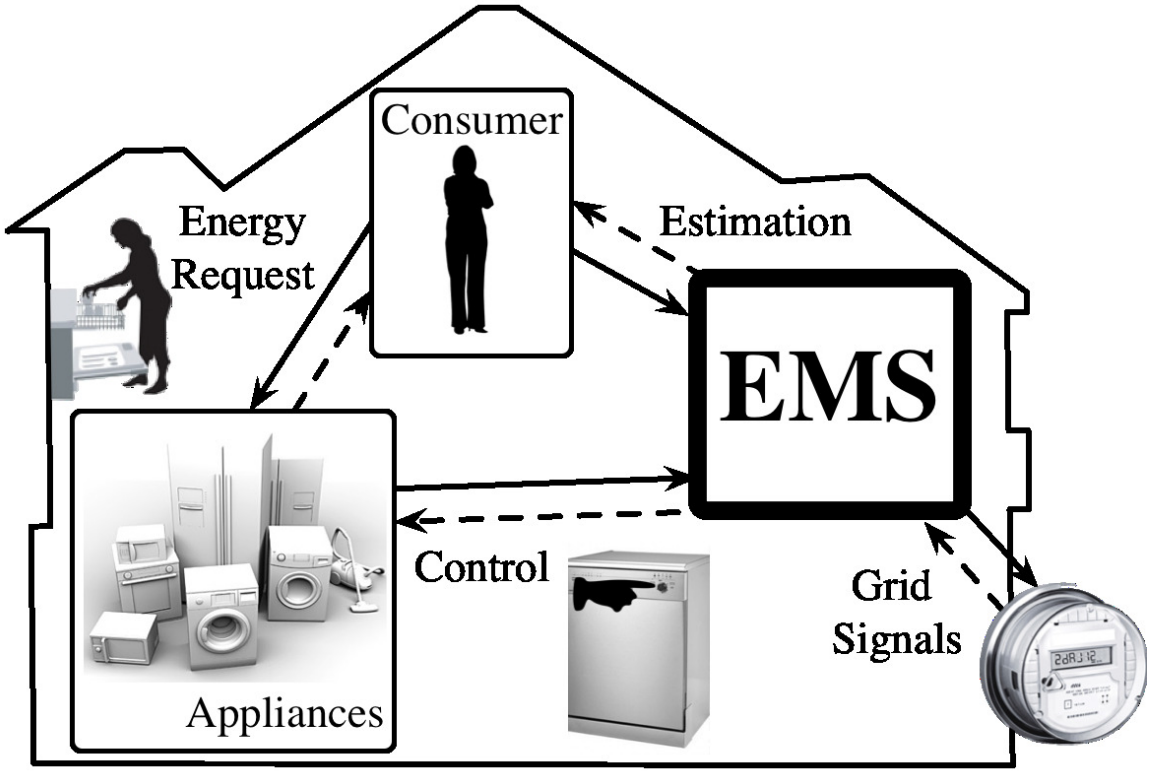

Figure 3.1: Consumer-centric Energy Management System

of the request, the EMS retrieves the present aggregate consumption as well as grid signals from the AMI. Given that the best fit behavioral sequence has already been detected, the EMS can predict future consumption states based on activity-dependent load inferences and compare these states to grid signals. The EMS calculates the likelihood that the additional requested load results in residential consumption in excess of the grid signal constraint for the duration of the requested appliance operational cycle. If the likelihood of the exceeding the grid signal is within an additional parameter defined by the user, the appliance is scheduled to run. If not, the load is deferred as the system waits for the next available time trial and AMI power consumption observation.

Table 3.1: Model Random Variables and Parameters

Random Variable	State Description	Parameters
A	daily activity	$P(A_{t+1}\|A_t)$
V^l	short-term appliance	$P\left(V^l_{t+1}\|V^l_t\right)$
C	$\sum_{l\in\mathcal{S}_{V^l\|A}} V^l_t$	$P(C_{t+1}\|C_t, A_t{=}a_i)$
E	shiftable appliance	$P\left(E_{t+1}\|E_t, A_t\right)$
F	non-shiftable appliance	$P\left(F_{t+1}\|F_t\right)$
Z	$Z_t = [A_t, C_t, E_t, F_t]^\top$	$P(Z_{t+1}\|Z_t)$
X	aggregate consumption	$X_t{=}C_t{+}E_t{+}F_t$

3.2 Stochastic Model

We can build a hierarchical model for the consumer as a vector-valued homogeneous Markov chain that includes activity and individual home appliance random variables corresponding to activity-appliance combinations discussed in Section 3.1. The Markov chain, by definition, is discrete in time and assumed to be discrete in state-space. Components of the vector valued chain are also assumed to behave Markovian. Each individual random variable used to construct the model is presented and summarized in Table 3.1.

3.2.1 Consumer Activity

We define a categorical random variable A of consumer activities as a homogeneous Markov chain, discrete in time and discrete in space $A{=}\{A_t{=}a_i, t, i{\in}\mathbb{N}^+\}$ where t is time, and a_i is an activity label from a finite set of outcomes in the state space $\mathcal{S}_A$. These activity labels or states include activities of daily living such as *dressing*, *dining*, etc. Since A is a temporal process representing a sequence of daily living activities, we structure A as a "left-right" non-ergodic (Bakis) chain where the state index

increases or stays the same as time increases. A is described by the transition matrix $P(A_{t+1}|A_t)$ which has the characteristics of being a $\max(\mathcal{S}_A) \times \max(\mathcal{S}_A)$ diagonal band sparse matrix with an absorbing terminal state $a_{\max(\mathcal{S})}$. The sequences of A are based on permutations of activities without repetition. These sequences terminate on particular activities (i.e. *sleep* or *leave*) to differentiate between times of day. For example, in the morning a consumer may wake up to perform *hygiene* tasks, *dress*, and *leave* for work, where *leave* represents the end of the morning sequence. Possible repeated activities such as *hygiene* or *dress* are enumerated and may have different permanence times described by self-looping probabilities in the Markov transition matrix of A which are adapted from (28; 29), and (30).

3.2.2 Taxonomy of Appliances

In accordance with the work presented in (31), we describe a taxonomy of the types of appliances present in the home.

- Activity-dependent short-term appliances
- Activity-dependent long-term "shiftable" appliances
- Activity-independent long-term "non-shiftable" appliances

We construct individual appliance Markov chains for each type based on the quantized Watt value of individual operating modes respectively. In other words, for a specific appliance, we identify discrete states based steady-state power consumption levels from sub-metered appliance curves and manufacturer specifications. Operational start and end times for each appliance are built in the Markov chain transition matrix. State transitions are estimated based on the frequency of transitions from one power level to another relative to the total number of transitions from the power

level under consideration as demonstrated in (32).

Dependent Short-term Appliances:

We define a random variable V^l, where $1 \leq l \leq L$ represents each short-term activity dependent device, with L total short-term appliances present in the home. $V^l = \{V_t^l = v_j, j, k, l \in \mathbb{N}^+\}$, described by the transition matrix $P\left(V_{t+1}^l | V_t^l\right)$ and state space $\mathcal{S}_{V^l}$. v_j, the state of V_t^l at any given time trial, is equal to the consumption value for the state of appliance l. We may partially build the vector-valued Markov chain for short-term appliances that depend on activity A as $[A_t{=}a_i, V_t^1{=}v_i^1, \ldots, V_t^L{=}v_i^L]^\top$, where $t \in \mathbb{N}^+$ and $a_i \in \mathcal{S}_A$, $v_i^1 \in \mathcal{S}_{V^1}$, and $v_i^L \in \mathcal{S}_{V^L}$. Short-term activity dependent devices are activated during specific behavioral activities. For example for the activity *cook*, the appliances stove, oven, toaster, coffee maker, blender would constitute short-term activity dependent appliances. While for the activity *workout*, dependent appliances would include the treadmill, elliptical machine, or stationary bicycle. However, for a large inventory of short-term devices, the vector-valued Markov chain grows quickly in complexity. In this context, as the number of appliances increase, the number of individual device states corresponding to consumption level increase directly affecting transition matrix dimensions as well as the number of mathematical operations used to calculate the forward probabilities described in Section 3.3. Complexity also becomes an issue when individual devices are assumed to operate with activation dependencies, as is the case with an entertainment system. In this example, turning on the television may also turn on the sound system, recording device, and the game console, requiring additional activation sub-chains to be encoded in the system model. For these appliance clusters, the state space can quickly become intractable. To alleviate complexity we note that the sum of the V_t^l for a time slice and affiliated

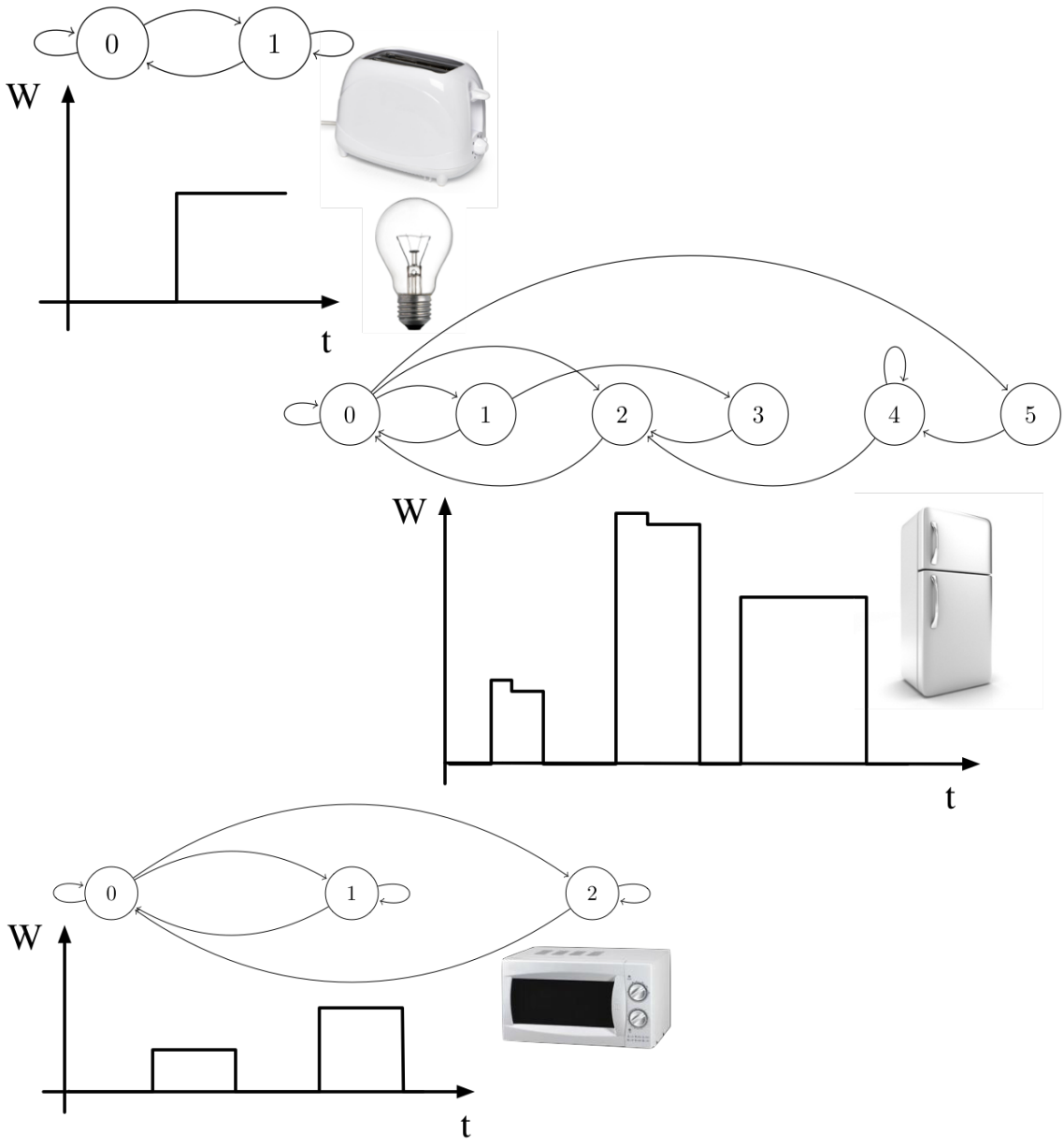

Figure 3.2: Appliance Markov chains.

activity results in a short-term appliance aggregate consumption. This allows us to compress the state space by defining the partially defined vector-valued Markov chain in terms of the random variable C, where we assume:

$$C_t = \sum_{l \in \mathcal{S}_{V^l|A}} V_t^l, \tag{3.1}$$

where $\mathcal{S}_{V^l|A}$ is the set of appliances involved in the activity. We can solve to get the elements of the transition matrix of C for a particular $A{=}a_i$ by

$$P(C_{t+1}, A_{t+1}{=}a_i | C_t, A_t{=}a_i) = P(C_{t+1} | C_t, A_t{=}a_i)$$

$$= P\Big(\sum_{l \in \mathcal{S}_{V^l|A}} V_{t+1}^l, A_t{=}a_i | \sum_{l \in \mathcal{S}_{V^l|A}} V_t^l, A_t{=}a_i \Big) \tag{3.2}$$

$$= \sum \prod_{l \in \mathcal{S}_{V^l|A}} P(V_{t+1}^l | V_t^l) \tag{3.3}$$

for a given activity $A = a_i$. Since we compress the state space by taking into account clusters of activity-dependent appliances defined by aggregate power consumption, appliance activation dependencies for a specific activity have no net effect, allowing us to achieve the same system model as when the devices are assumed to activate independently. When $A_{t+1}{=}a_j \neq A_t{=}a_i$ we use the stationary distribution

$$\lim_{n \to \infty} \frac{1}{n} \sum_{m=1}^{n} P(C_m, | C_0, A_0{=}a_j) \tag{3.4}$$

as the initial distribution of moving into the new activity and appliance dependencies. The state space $\mathcal{S}_C$, is defined by states c_j, where $j = \{1, \ldots, \prod_{i=l}^{L} \max \mathcal{S}_{V^i}\}$

Dependent Long-term "Shiftable" Appliances:

We are interested in scheduling these appliances with our control agent. "Shiftable" otherwise known as deferrable loads are characterized by long operational cycles, high load profiles, and function without interruption once activated. These appliances are dependent on activity A. Examples of "shiftable" activity-dependent loads are the washing machine and the dishwasher which are likely initiated when the user is in the activity state "clean." In our model we define these loads as E=$\{E_t$=$e_m, k, m \in \mathbb{N}^+\}$, described by the transition matrix $P\left(E_{t+1}|E_t, A_t\right)$ and state space $\mathcal{S}_E$. The transition matrix is characterized by the operation time spent in each power state. Once initiated for an activity sequence, a memory variable is toggled between 1 and 0 to keep track of a finished appliance cycle. These appliances are not included in the vector-valued chain, but the "shiftable" appliances that the user may not seek to control, are included. For generality, we will include a "shiftable" appliance for both the controlled and uncontrolled case.

Independent Long-term "Non-shiftable" Appliances

"Non-shiftable" or non-deferrable loads are loads which operate irrespective of the activity and are essential for the proper function of the home. For example a refrigerator must always be on to ensure the safety and quality of food for the inhabitant. These loads are not controlled by the energy management system as they must operate at all times. $F = \{F_t = v_t, k, n \in \mathbb{N}^+\}$, is described by the transition matrix $P\left(F_{t+1}|F_t\right)$ and state space $\mathcal{S}_F$.

3.2.3 The Complete Model

We now proceed to define the model in its entirety, based upon the definitions of random variables A, C, E, and F. The vector-valued Markov chain $Z_t{=}[A_t{=}a_i, C_t{=}c_i, E_t{=}e_i, F_t{=}f_i]^\top$, where $t{\in}\mathbb{N}^+$ represents the hidden state and the observation $X_t{=}C_t{+}E_t{+}F_t$ is the aggregate residential consumption. To fully characterize the HMM transition matrix $P(Z_{t+1}|Z_t) = P(A_{t+1}, C_{t+1}, E_{t+1}, F_{t+1}|A_t, C_t, E_t, F_t)$ we use the chain rule.
For $A_{t+1}{=}A_t$, $P(Z_{t+1}|Z_t){=}$

$$P(A_{t+1}|A_t)P(C_{t+1}|C_t,A_t)P(E_{t+1}|E_t,A_t)P(F_{t+1}|F_t). \tag{3.5}$$

For $A_{t+1}{\neq}A_t$, $P(Z_{t+1}|Z_t){=}$

$$P(A_{t+1}|A_t)\Pi_C(i, A_{t+1})\Pi_E(j, A_{t+1})P(F_{t+1}|F_t), \tag{3.6}$$

for $1{\leq}i{\leq}\max(\mathcal{S}_C)$ and $1{\leq}j{\leq}\max(\mathcal{S}_E)$. Π_C and Π_E are the initial distribution of the aggregate consumption of the short-term activity dependent appliances and the initial distribution of the single activity dependent "shiftable" long-term appliance. The element-wise initial distribution of the HMM is

$$\begin{aligned}\Pi_{Z_1}&{=}\Pi_{A_1,C_1,E_1,F_1}\\ &{=}\Pi_A(A_1{=}a)\Pi_C(i, A_1)\Pi_E(j, A_1)\Pi_F(k).\end{aligned} \tag{3.7}$$

for $1{\leq}a{\leq}\max(\mathcal{S}_A)$, $1{\leq}i{\leq}\max(\mathcal{S}_C)$, $1{\leq}j{\leq}\max(\mathcal{S}_E)$, $1{\leq}k{\leq}\max(\mathcal{S}_F)$. The emission matrix is defined as:

$$P(X_t|Z_t) = P(X_t|A_t, C_t, E_t, F_t). \tag{3.8}$$

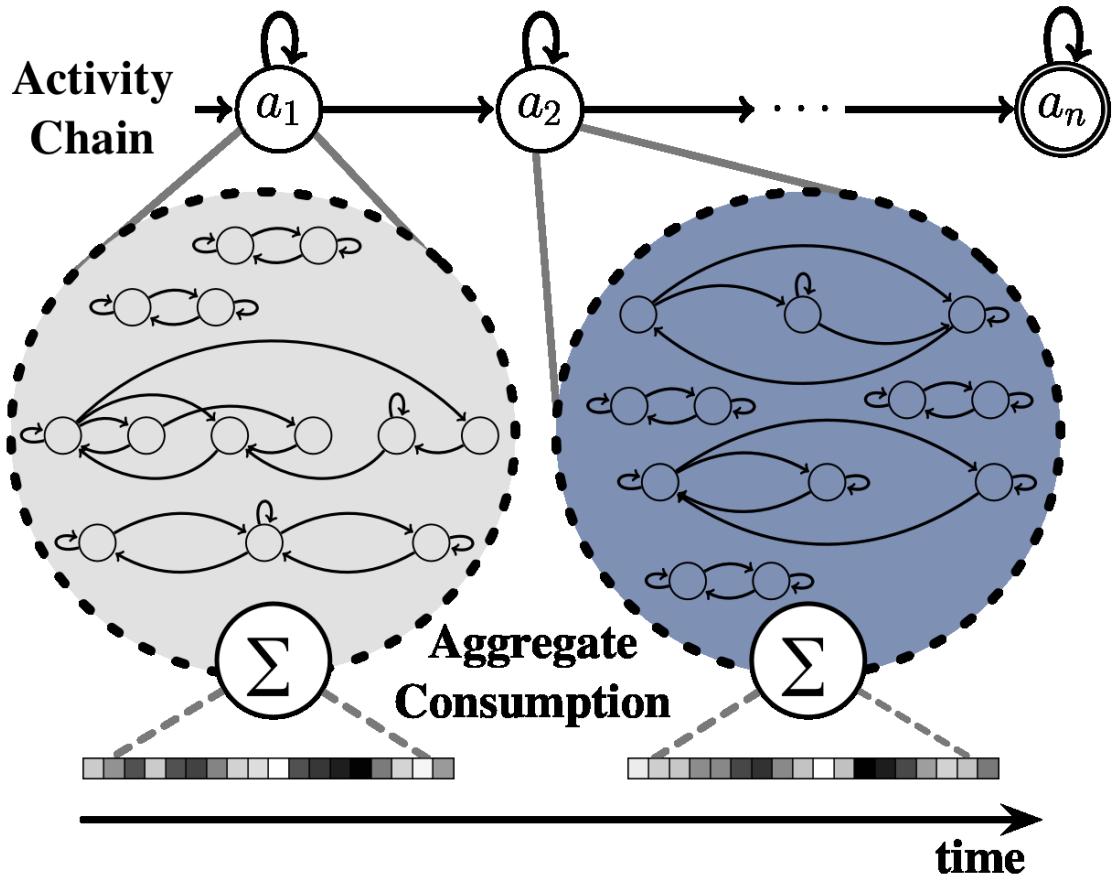

Figure 3.3: Activity appliance dependencies, including short-term,"shiftable," and "nonshiftable" loads which sum to the total consumption per time slice.

The emission matrix is built by identifying which combinations of C_t, E_t, and F_t result in the observation X_t=C_t+E_t+F_t. This matrix has dimensions of $\max(\mathcal{S}_Z) \times \max(\mathcal{S}_X)$.

3.3 Model and State Detection

The proposed energy management control agent operates by detecting and classifying the resident into a particular reference model λ_i defined by $(\Pi_Z^{(i)}, P(Z_{t+1}^{(i)}|Z_t^{(i)}), P(X_t|Z_t^{(i)}))$ for $1 \leq i \leq \max(\mathcal{S}_{\lambda_i})$ from a dictionary of models based on the time of day, within a training period T. The set of possible models are derived from unique sequences

of activities A corresponding to possible consumer schedules and employment demographics. Different sequences result in different activity transition probabilities, $P(A_{t+1}^{(i)}|A_t^{(i)})$, which are propagated to the calculations of $\Pi_Z^{(i)}$, $P(Z_{t+1}^{(i)}|Z_t^{(i)})$, and $P(X_t|Z_t^{(i)})$ used to define a specific λ_i as outlined in Section 3.2. Following the training period T, the identified model λ_i is used to calculate the maximum likely current joint state of total home appliances and activity Z_t which allows the system to predict the likelihood of future consumption observations for a rolling time horizon. The resulting load profile predictions inform real-time decisions with respect to the scheduling of "shiftable" loads in light of consumption limits defined by demand response and user comfort discussed in Section 3.4. In order to calculate the best fit reference model, λ_i for a consumer we utilize the forward algorithm for HMMs to calculate the posteriori probability based on a sequence of consumption observations during the training period T.

3.3.1 Consumer Model Detection

Given the observation sequence: $X_1{=}x_j, \ldots, X_T{=}x_z$, we may calculate:

$$\alpha_k(s){=}P(X_1{=}x_j, \ldots, X_T{=}x_z, Z_k{=}s)$$

for a specific model λ_i defined by

$$(\Pi_Z^{(i)}, P(Z_{t+1}^{(i)}|Z_t^{(i)}), P(X_t|Z_t^{(i)}))$$

or in matrix format: $(\mathbf{\Pi}_{\lambda_i}, \mathbf{P}_{\lambda_i}, \mathbf{B}_{\lambda_i})$. For the first time step we calculate the probability of the joint distribution of the first hidden state and consumption observation using the initial distribution of the hidden chain. $\alpha_1^{(i)}(s){=}P(X_1{=}x_j, Z_1^{(i)}{=}s) =$

$\Pi_{Z_1}^{(i)}(s)P(X_1{=}x_j|Z_1^{(i)}{=}s)$, or

$$\alpha_1^{(i)}{=}\mathbf{\Pi}_{\boldsymbol{\lambda_i}}^{\top} \cdot \mathbf{P}_{\lambda_i}. \tag{3.9}$$

We may generalize the remaining forward calculations for $1{\leq}t{\leq}T-1$ as

$$\alpha_{t+1}^{(i)}{=}\alpha_t^{(i)} \cdot (diag(\mathbf{B}_{X_{t+1=x}})_{\lambda_i}) \cdot \mathbf{P}_{\lambda_i}. \tag{3.10}$$

To classify the user we evaluate

$$\sum_{r \in \mathcal{S}_{Z^{\lambda_i}}} \alpha_T^{(i)}(r), \tag{3.11}$$

where T is the training period. The model λ_i that results in the maximal value is then identified as the approximate user reference class based on the sequence of real-time observations sensed by the system.

3.3.2 State Estimation based on Model

Once a reference class for a sequence of training observations $X_1{=}x_j, \ldots, X_T{=}x_z$, is determined ($\lambda_i{=}\lambda$), the state estimate may be calculated by propagating the forward a posteriori probability value for the new real-time consumption observations using the statistics, $(\mathbf{\Pi}_\lambda, \mathbf{P}_\lambda, \mathbf{B}_\lambda)$, of the reference class. Since we have identified the best fit model according to the resident's consumption, we drop the λ_i in our notation in this section to increase readability. We can scale the forward joint probability value to obtain a distribution of states. In other words, given the sequence $X_{T+1}{=}x_a \ldots, X_t{=}x_b$

we are interested in calculating

$$P(Z_t{=}s|X_{T+1}{=}x_a,\ldots,X_t{=}x_b){=}\frac{\alpha_t(s)}{\sum\limits_{r\in\mathcal{S}_Z}\alpha_t(r)}. \tag{3.12}$$

The state $Z_t{=}s$ that results in the greatest probability given the observation sequence is defined as the maximum likelihood estimate.

3.4 Control

An "on/off" appliance control algorithm is developed based on consumer classification and the current hidden state estimate to determine the soonest available time slice to schedule "shiftable" must-run loads under consumption and user-defined constraints.

3.4.1 Grid Signals

We represent a consumption constraint z, a maximum Watt value, which may be a function of utility pricing programs or grid alerts. To schedule a deferrable load we must compare the sensed current user consumption, X_t, with the constraint as well as the energy use profile of the deferrable load itself. In this scheme, the "shiftable" load profile is deterministic as it follows a defined operational cycle, d_t, for $1 \leq t \leq N$ upon activation. We are interested in calculating:

$$P(X_t \geq z - d_t),$$

which corresponds to the joint state $Z_t{=}(A_t, C_t, E_t, F_t)$ for the combinations of C_t, E_t, F_t that produce a total wattage in excess of the consumption constraint $z - d_t$. We can thereby partition the state space of Z_t into two sets, the "taboo" set, H_Z correspond-

ing to $X_t = C_t + E_t + F_t \geq z - d_t$, and its complement H_Z^{c}. We then rearrange the states of $P(Z_{t+1}|Z_t)$ to the following format:

$$P(Z_{t+1}|Z_t) = \begin{bmatrix} \mathbf{T_Z}(\mathbf{1},\mathbf{1}) & \mathbf{T_Z}(\mathbf{1},\mathbf{2}) \\ \mathbf{T_Z}(\mathbf{2},\mathbf{1}) & \mathbf{T_Z}(\mathbf{2},\mathbf{2}) \end{bmatrix} \tag{3.13}$$

where $\mathbf{T_Z}(\mathbf{1},\mathbf{1})$ represents the sub-matrix of states which transition from $H_Z^{\mathsf{c}} \rightarrow H_Z^{\mathsf{c}}$, $\mathbf{T_Z}(\mathbf{1},\mathbf{2})$ represents the sub-matrix of states which transition from $H_Z \rightarrow H_Z^{\mathsf{c}}$, $\mathbf{T_Z}(\mathbf{2},\mathbf{1})$ represents the sub-matrix of states which transition from $H_Z^{\mathsf{c}} \rightarrow H$, and $\mathbf{T_Z}(\mathbf{2},\mathbf{2})$ represents the sub-matrix of states which transition from $H_Z \rightarrow H_Z$ (24).

The total probability of transitioning from H_Z^{c} to the set H_Z within a finite time horizon, N, defined by the operational cycle of d_t, can be calculated using the sub-matrices of the rearranged transition matrix as

$$P_{\mathbf{T_Z}(\mathbf{1},\mathbf{2})}(N) = \sum_{s \in \mathcal{S}_H} \sum_{n=1}^{N} \mathbf{T_Z}(\mathbf{1},\mathbf{1})^{n-1} * \mathbf{T_Z}(\mathbf{1},\mathbf{2}). \tag{3.14}$$

This probability provides the energy management system a means of predicting the user consumption profile for a finite time horizon, N, as well as a probability measure as with respect to the consumption constraint.

3.4.2 User Convenience

We can further implement an additional degree of freedom over the control of scheduling by taking into account user convenience defined by q which is a constraint placed on the probability of transitioning from H_Z^{c} to the set H_Z within the operational cycle of the appliance we seek to control. In other words, the consumer convenience constraint allows the user to loosen the grid defined consumption constraint by allowing

the resident consumption to hit states above threshold $z - d_t$ within a probability of q. In other words,

$$P_{\mathbf{T_Z(1,2)}}(N) = \sum_{s \in \mathcal{S}_H} \sum_{n=1}^{N} \mathbf{T_Z}(\mathbf{1},\mathbf{1})^{n-1} * \mathbf{T_Z}(\mathbf{1},\mathbf{2}) \leq q \tag{3.15}$$

Thus, the user has the ability to tune the tradeoff between convenience and consumption threshold rules, affecting the resulting delay in activating the appliance.

3.4.3 Control Algorithm

We outline the control algorithm based on activity sequence detection from a library of typical user reference models, state estimation based on the detected model and current consumption, and the evaluation of energy requests constrained by grid signals and user convenience.

- A sequence of real-time resident consumption observations are input to the EMS via the "smart" meter. For a training period of T, we use the forward algorithm to calculate the a posteriori probability for a set of typical reference models λ_i. Following the training period, the model resulting in $\max(\sum_{r \in \mathcal{S}_{Z^{\lambda_i}}} \alpha_T(r))$, is determined to be the closest approximate reference model.

- Based on the selected user model, we calculate the

$$\max(P(Z_t{=}s|X_{T+1}{=}x_a, \ldots, X_t{=}x_b)) = \max \frac{\alpha_t(s)}{\sum_{r \in \mathcal{S}_Z} \alpha_t(r)}$$

  to find the maximum likely state of the hidden Markov chain, Z_k for X_k following the training period.

- The consumer energy request $R_k = r$ where $r \in \{0, 1\}$ is dependent on the

activity $P(R_k|A_k)$. $R_k = 1$, represents the request being made, while $R_k = 0$ is no request. For each sequence of consumption observations, the request, once made cannot be repeated for the next time trial or appliance. In other words, once $R_k = 1$, the request cannot be made again.

- Based upon R_k and the state estimate of Z_k at the time of the request k, we determine if the state $Z_k \in H_Z$. If it is in the "taboo" set we wait to update the state estimate for the next time trial until the state is no longer "taboo." Once $Z_k \in H_Z^{\mathsf{c}}$, we find the total probability of hitting the set H_Z given that we started in a "safe" set.

- Activation of the appliance occurs when the total probability, $P_{\mathbf{T_Z(1,2)}}(N) \leq q$ of hitting the set H_Z given that we started in H_Z^{c}.

3.5 Numerical Results

We present the results of an EMS case study for an evening time of day sequence of activities comprised of one hundred fifty discrete time trials with each time trial representing a five minute interval. The individual activity A and the household inventory of short-term appliances V^l is presented in Table 3.2. With the appliance inventory, the reference models, $\lambda_1 \sim (\Pi_{Z^{(1)}}, P(Z_{t+1}^{(1)}|Z_t^{(1)}), P(X_t|Z_t^{(1)}))$, $\lambda_2 \sim (\Pi_{Z^{(2)}}, P(Z_{t+1}^{(2)}|Z_t^{(2)}), P(X_t|Z_t^{(2)}))$, and $\lambda_3 \sim (\Pi_{Z^{(3)}}, P(Z_{t+1}^{(3)}|Z_t^{(3)}), P(X_t|Z_t^{(3)}))$ used for model detection and state estimation are:

Evening Model 1/PM1 (λ_1): This model is derived from the activity sequence $A^{(1)}$= *hygiene, dress, cook, dine, clean, rest,* and *sleep.*

Evening Model 2/PM2 (λ_2): This model is derived from the activity sequence $A^{(2)}$= *hygiene, dress, leave, hygiene, dress,* and *sleep.* We differentiate repeated

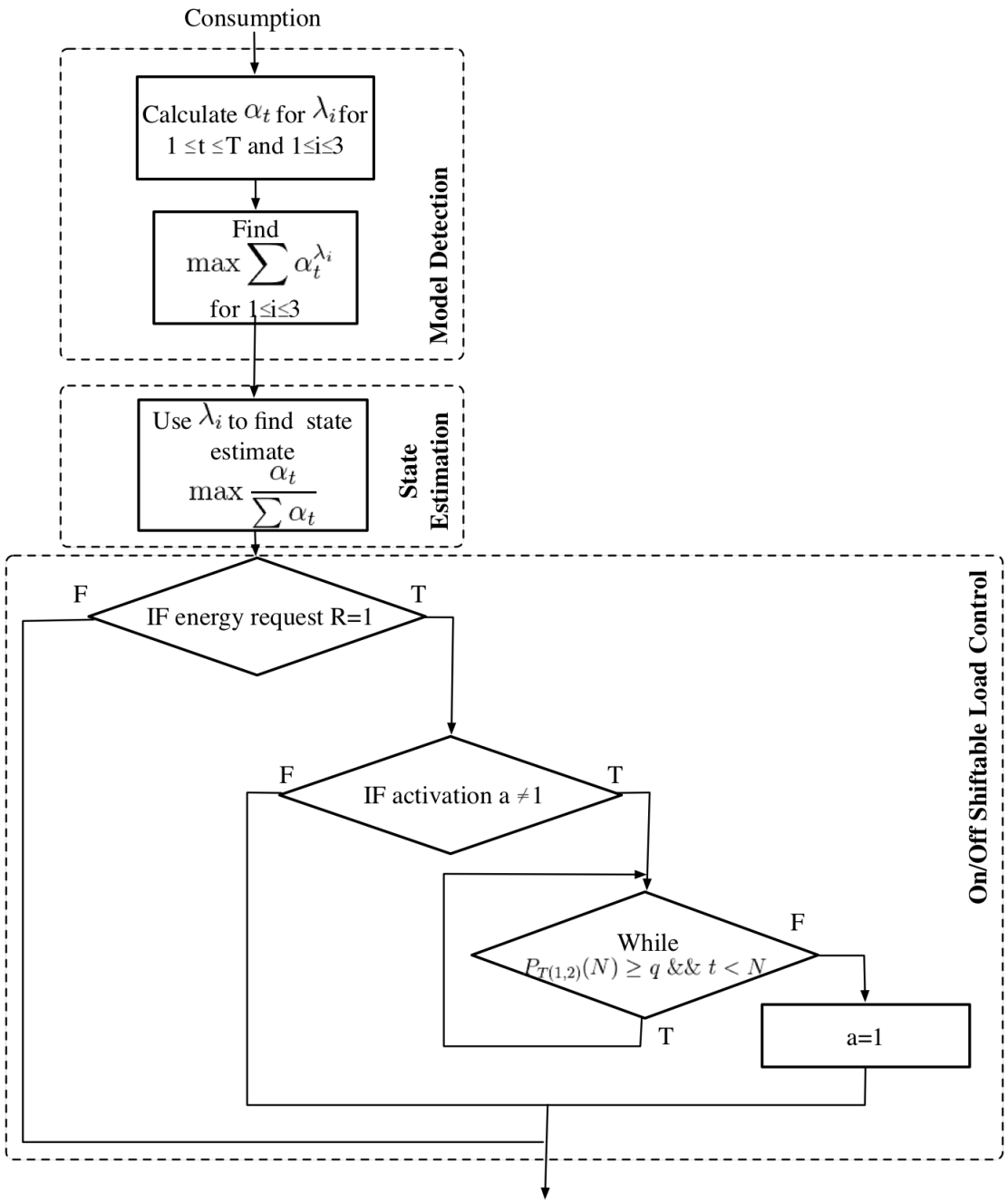

Figure 3.4: Control Algorithm Flow chart.

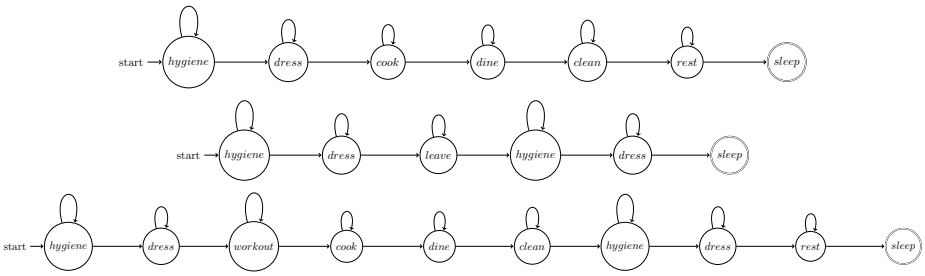

Figure 3.5: Evening reference models: sequences of activities, PM1, PM2, and PM3.

activities as separate states with different self-looping state probabilities and characteristics. For example *hygiene* following the state *leave* may be longer in duration than *hygiene* upon arrival.

Evening Model 3/PM3 (λ_3): This model is derived from the activity sequence $A^{(3)}$= *hygiene, dress, workout, cook, dine, clean, hygiene, dress, rest,* and *sleep.*

To benchmark performance, reference model λ_1 is used to generate 100 sample functions, or aggregate consumption sequences over $1 \leq k \leq 150$ time trials. We keep track of the hidden joint state $Z_t = A_t, C_t, E_t, F_t$, as well as the visible consumption emitted by the chain, $X_t = C_t + E_t + F_t$. For each sequence, we use a random function to generate a request R_t as a function of activity $P(R_t|A_t)$. For this study we set the grid alert consumption constraint to z = 5kW and examine the effects of the consumer parameter by analyzing system performance for $0 \leq q \leq 1$.

3.5.1 Model Detection Performance

Using reference models λ_1, λ_2, and λ_3 to seed and generate three sets of 100 sample functions, we test the performance of the forward algorithm in detecting the best fit model. As described in section 3.3, we evaluate the $\alpha_k(s)$ statistics along all states with respect to the model parameters of λ_1,λ_2, and λ_3 for a single sample function. We then calculate the sum, $\sum_{s \in \mathcal{S}_{\vec{Z}}^{\lambda}} \alpha_k(s)$, along all states for each model and for each time trial in the sample function. We compare the value amongst all models considered.

Table 3.2: Activities and dependent short-term appliances with associated wattage.

Activity	**Dependent Devices**	**Range (W)**
leave	alarm, lights	$0 - 1000$
hygiene	electric water heater, hairdryer, lights	$0 - 5000$
dine	toaster, microwave, lights	$0 - 3700$
rest	tv, lights	$0 - 650$
workout	treadmill, tv, lights	$0 - 2650$
dress	iron, lights	$0 - 1600$
clean	electric water heater, vacuum, lights	$0 - 4000$
sleep	alarm, lights	$0 - 1000$
cook	toaster, stove, coffeemaker, microwave, lights	$0 - 7500$

Table 3.3: Long-term appliances, taxonomy, and associated wattage.

Appliance	**"Shiftable"**	**Range (W)**
electric vehicle supply (EVSE)	yes	$0 - 12000$
heating and air conditioning (HVAC)	yes	$0 - 40000$
dishwasher	yes	$0 - 1500$
refrigerator	no	$0 - 400$

Table 3.4: Model Detection: Time to 90% Confidence Levels

Evening Model	**Interpolated Time Trial**	**Minutes**
λ_1 (PM1)	7.3332	36.6660
λ_2 (PM2)	1	5
λ_3 (PM3)	9.6660	48.3300

The model that results in the maximum value of $\sum_{s \in \mathcal{S}_{\vec{Z}}^{\lambda}} \alpha_k(s)$ is the "best fit model" for that particular time trial. We repeat this process for all 100 samples generated by an individual seed model to validate the accuracy of the model detection algorithm. To produce figure 3.6 for each time trial in a single sample function we calculate the detection frequency of each model and repeat the process for the set of 100 sample functions seeded by the model parameters under consideration.

We are interested in studying the rate of convergence of correct model detection for each seed model which differ relative to one another based on the sequence and duration of behavioral activities. For example, evening model 2, or λ_2, is detected with a confidence exceeding 90% by the first time trial. This is due to the fact that the user *leaves*, which is an activity unique to λ_2 relative to λ_1 or λ_3. Furthermore, this particular model has a load characteristic influenced by the electric vehicle supply equipment (EVSE) fast-charging operation mode, followed by a period of little consumption during the activity *leave*. As shown in table **??**, λ_1 is detected with over 90% confidence by the 8th discrete time trial corresponding to 40 minutes. λ_3 is detected with over 90% confidence by the 10th discrete time trial corresponding to 50 minutes into the activity sequence. The rate of convergence between λ_1 and λ_3 may be due to structural similarities between models as well as activity sequences that have comparable consumption profiles. Thus, to achieve model detection within 90% confidence requires longer training periods depending on the model similarity.

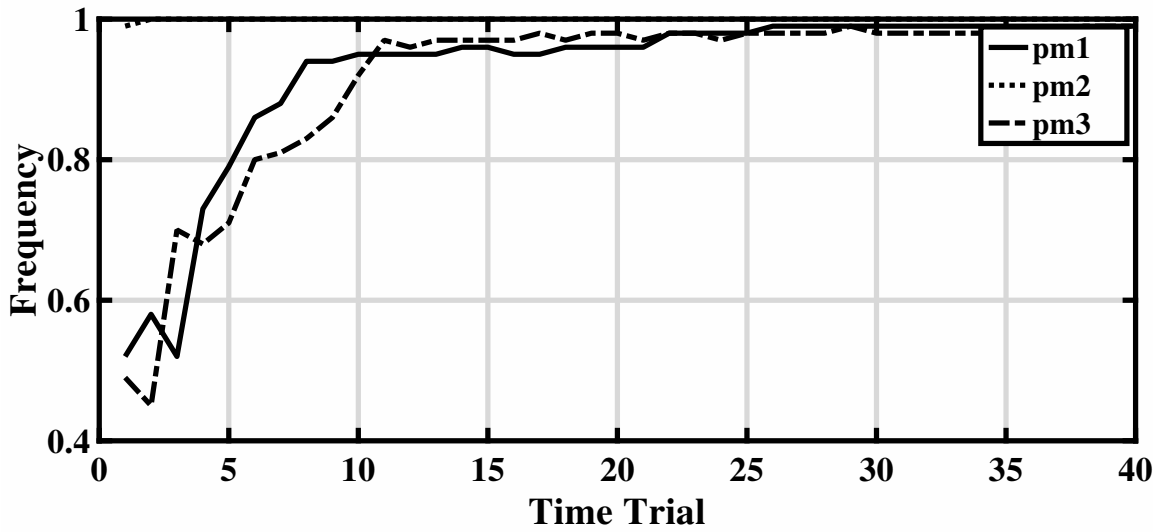

Figure 3.6: Probability of detecting correct model for respective self-seeded sample functions.

3.5.2 Activity Influence on Consumption

To demonstrate the influence of human behavioral activity on load profile we examine the total consumption for the inventory of short-term and long-term appliances presented in tables 3.2 and 3.3 for individual human activities. For sake of clarity we present the expected consumption of two behavioral activities which can easily be extended to many. Figure 3.7 shows the expected consumption for the activities *cook* and *rest* for a time horizon of 5 trials corresponding to 25 minutes following the detection of the current wattage observation at time trial $t = 0$. The expected value for each activity is calculated by taking advantage of the hierarchical structure of each individual activity in terms of the activity dependent short-term devices and the activity dependent and independent long-term devices. We then examine the individual activity Markov chains which are homogeneous and discrete in state space allowing us to take advantage of the Chapman-Kolmogorov equations expressed as matrix multiplications describing the distribution of moving from the state at $t = 0$ to other states. Knowing the distribution allows us to calculate the expected consump-

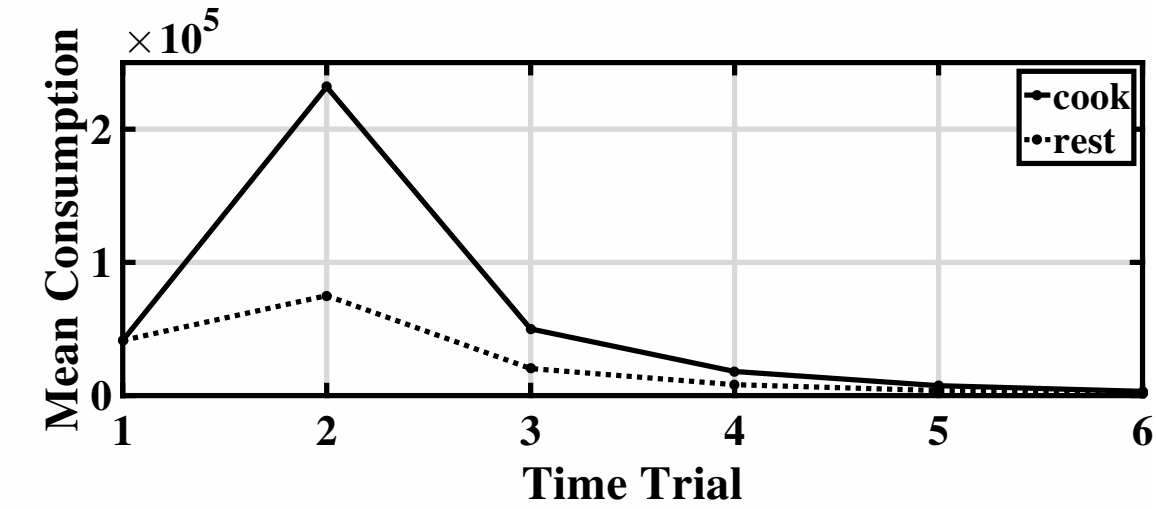

Figure 3.7: Expected consumption over a time horizon of 5 trials for activities 'cook' and 'rest.'

tion value by weighting the distribution with the discrete wattage value of each state, thereby obtaining the mean consumption at each time trial in the horizon considered. Note at time trial $t = 0$, the activities *cook* and *rest* both produce a total consumption observation of 41.4 kW. However, after time $t = 0$, *cook* and *rest* result in very different expected consumption observations. This is because *cook*, while producing a wattage observation of 41.4 kW, contributes to larger consumption observations due to additional appliance dependencies that *rest* does not include as illustrated in table 3.2. Since the expected consumption is a function of the matrix multiplication form of the Chapman-Kolmogorov equations, with time the distribution decreases and reaches the stationary distribution for each individual activity.

3.5.3 Activity-Informed Control

We study the resulting scheduling control of the EMS for a sample function seeded by λ_1 as outlined in the procedure. Figure 3.8 presents a single sample function selected from the set of 100 simulations seeded by the model parameters of λ_1, also known as

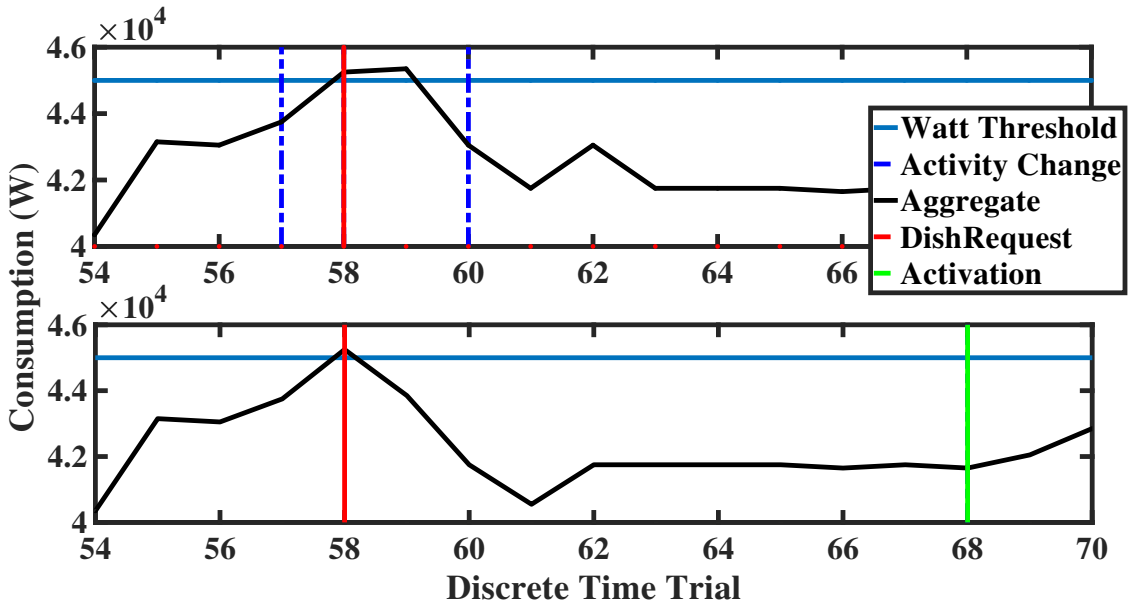

Figure 3.8: Dishwasher scheduling comparison of visible Markov chain with detected model and estimated state.

PM1. We select this particular sample to demonstrate the robustness of our control framework with respect to aggregate consumption and appliance scheduling despite inaccuracies in activity detection. In figure 3.8, we illustrate a case where the user prioritizes consumption constraints over appliance activation resulting in activation delay. The consumption constraint, labeled as "watt threshold," is representative of a pricing threshold via tiered pricing programs set by the utility. For example, the watt threshold may indicate a pricing shift from baseline to medium or peak consumption allowance. The cost savings would then be directly proportional to the reduction of time spent above the pricing defined consumption threshold. The first subplot of figure 3.8 shows the evening behavior of the user without the proposed energy management system (EMS). At the $t = 58$ time trial following behavior model detection outlined in section 3.3, the user requests dishwasher activation. Since there is no EMS in place the dishwasher is activated upon request resulting in a load profile exceeding the consumption threshold from $t = 57.83$ to $t = 59.14$. This threshold is indicative of a specific tiered pricing program.Since tiered utility pricing programs

vary with respect to location and region, we generalize our simulations to a consumption threshold which can be adapted to pricing depending on the utility provider. In the case of dynamic or time of use pricing, the consumption threshold represented as a constant would be replaced by a function specific to market demand or utility pricing respectively. In the second subplot of figure 3.8, the identical activity influenced load profile featured in the first subplot is considered under the control of the EMS wherein we demonstrate control over the single appliance *dishwasher*. The user similarly requests activation of the dishwasher at $t = 58$ time trial. In this subplot, the consumption threshold is exceeded from $t = 57.83$ to $t = 58.18$. However, we notice that the time spent above threshold is less than in the case without the EMS. In other words, irrespective of the scheduling request to activate the dishwasher, at time trial $t = 58$, the system was headed in an aggregate consumption condition in excess of the the consumption threshold set at 45kW. Following the request at $t = 58$, the EMS takes into account the probability of exceeding the consumption threshold level for the next 5 time trials and waits until the probability is low. In the fully visible Markov chain in the first subplot of figure 3.8, the household consumption, including the tagged changes in behavior at time trial $t = 57$ and time trial $t = 60$ are provided. In the hidden Markov chain, both of these human behavior activity transitions are not detected. In figure 3.9 we observe the likelihood of a particular human behavioral activity at each given point in time. At $t = 57$, there is a 0.7288 probability of the activity being *cook* following $t = 56$ where *cook* was detected with a high probability of 0.9948. At $t = 57$, there is a .2532 probability of the current activity being *dine* and an even smaller probability of 0.018 of the current activity being *clean*. Therefore, at $t = 57$ the maximum likelihood estimate of human behavioral activity is determined to be *clean* which remains unchanged from the detected behavioral activity of the previous time trial. Furthermore, at time trial $t = 60$, the maximum likelihood estimate determines *cook* to once again be the current ac-

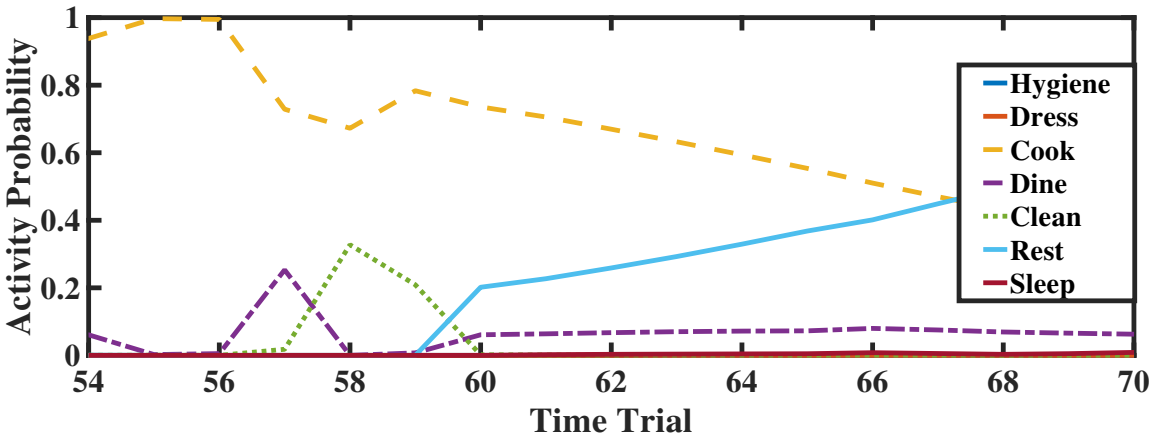

Figure 3.9: Single sample function activity probability.

tivity with a probability of 0.7356 in contrast to the 0.2017 probability of *rest* and the 0.06097 probability of *dine*. Once again the results reflect that the framework makes reasonable estimates on the current activity based on aggregate consumption characteristics using the maximum likelihood despite some inaccuracies in detecting changes between states that may display similar load profiles. However, in later time trials beyond $t = 66$ we see the activity *rest* increasing in probability which illustrates that though the HMM framework may not detect behavioral activity at a high resolution, after some time and updated observations, the correct behavioral activity will be detected with some delay which influences the scheduling EMS control system.

The goal of the study is to utilize human behavior schedules to infer demand for a rolling time horizon in order to schedule appliances under consumption constraints defined by utility pricing and consumer preferences. In the case where consumption thresholds are prioritized over consumer comfort with respect to appliance activation delay, the control mechanism schedules the dishwasher to run at time trial $t = 68$, 50 minutes following dishwasher appliance activation request. Figure 3.8 shows the scheduling and the resulting aggregate power consumption following dishwasher activation at a time of low load demand.

3.5.4 Comfort Consumption Tradeoff

We present the results of a simulation study that takes into account the consumer comfort level in terms of the activation delay with respect to appliance requested as well as the consumption threshold constraint. This study differs from previous work in that the activity informs the future consumption values for a time horizon that is dependent on the operational cycle of the appliance being controlled. In this study we continue to study the control of the dishwasher in terms of the delay in appliance activation given consumer comfort and the expected time in units of time trials, where each time trial represents 5 minutes, of the aggregate consumption exceeding the consumption threshold of 45kW. From figure 3.10 we examine the delay in appliance activation as a function of the consumer comfort parameter we have generalized as "probability threshold." In these results, taken over 100 sample functions for 1001 probability thresholds ranging from $0 - 1$ in uniform increments we compare and contrast the performance results of the fully visible Markov chain with the hidden Markov chain detected by the EMS framework. We see that the relationship occurs in discrete steps which is the result of the discrete construction of the chain and an effect of its Bakis characteristics. However, we see that the hidden Markov chain performs relatively well with respect to the fully visible chain but degrades for probability "comfort" values between 0.363 to 0.576 indicating premature activation of the appliance. To examine how the premature activation of the appliance affects the consumption threshold constraint we plot the mean time above the consumption threshold of 45 kW with respect to the probability threshold and again examine the results obtained for probability "comfort" values within this range. In figure 3.11 we notice within the window of "comfort" probability thresholds from 0.363 to 0.576, the EMS early activation, unsurprisingly results in larger times above 45kW consumption threshold. This is due to the fact that the HMM framework has less information

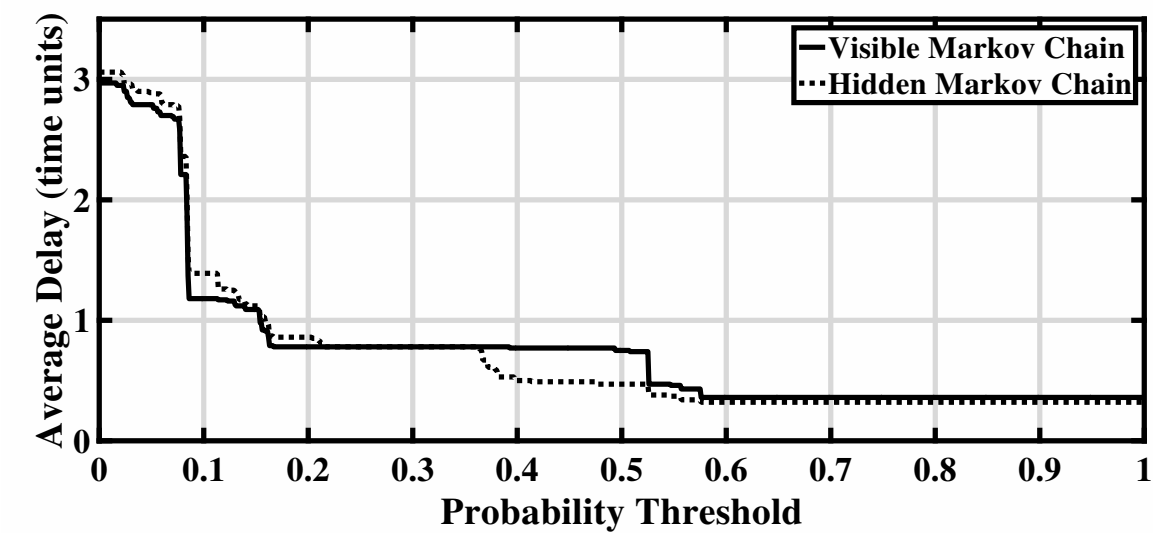

Figure 3.10: Appliance activation delay as a function of q.

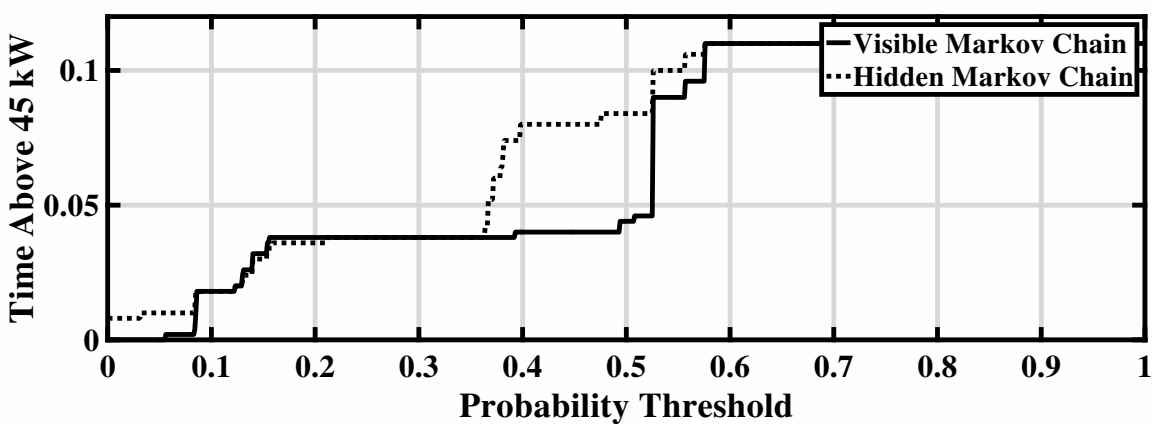

Figure 3.11: Average time above $X_t \geq 45$kW.

that the fully visible chain resulting in some degree of error that may be inherent to the simulation. In real systems, increased sample data with respect to consumption and behavioral activity on a daily basis offers some alleviation. The tradeoff between the average discrete time spent above consumption threshold as a function of delay is presented in 3.12. We see that the time spent above the 45kW is inversely proportional to the average activation delay calculated across the "comfort" probability constrained sample functions. In other words, the "comfort" probability allows a degree of freedom for the consumer in terms of choosing device activation irrespective of the consumption threshold set by the EMS.

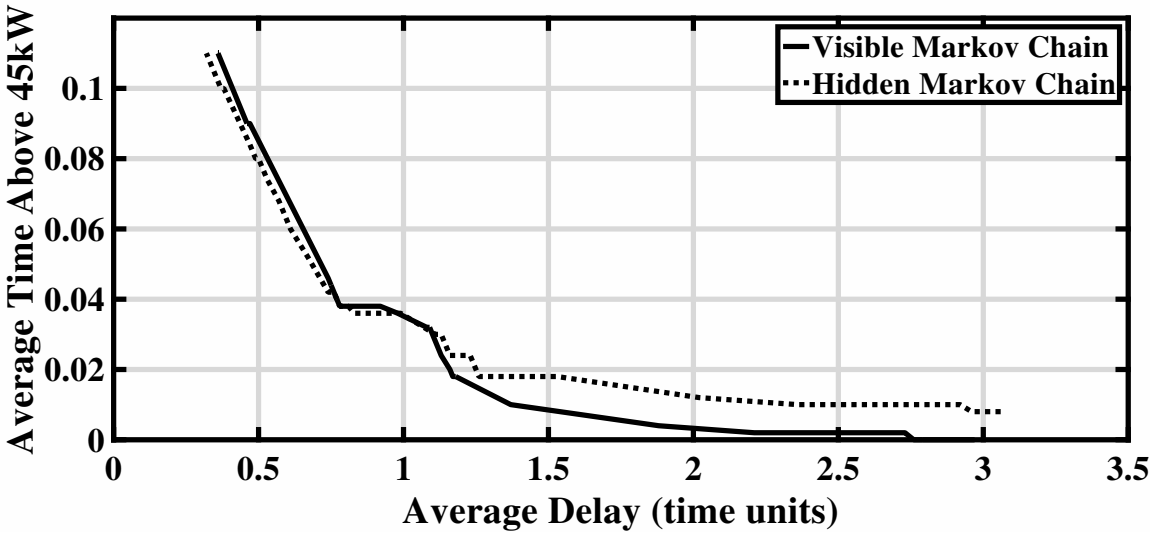

Figure 3.12: Average time above $X_t \geq 45$kW as a function of delay.

Chapter 4

Distributed Residential Generation and Storage

4.1 Distributed Energy Resource Management

The residential energy management system while scheduling appliances, must take into account distributed energy resources that the home owner may seek to use as an alternative source of energy or to supplement the energy provided by the utility. The agent must therefore sense current environmental parameters to determine whether the energy stored in the battery should be used to supply the power drawn by the load during high energy pricing, or whether to charge the battery during high incoming energy from residential microgeneration sources. The components of the distributed energy resource management subsystem of the home energy management system are introduced in Figure 4.1.

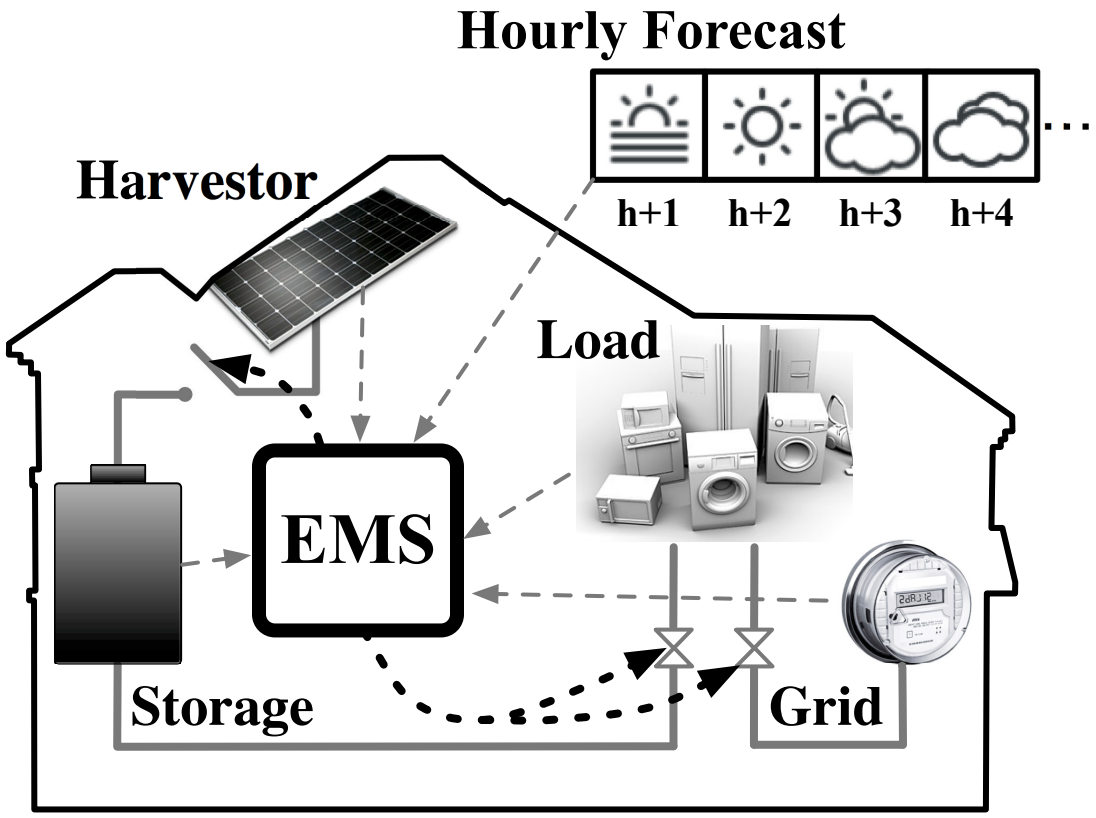

Figure 4.1: EMS overview for energy resource management and storage.

4.2 System Overview

4.2.1 The Harvestor

The energy harvesting device represents the available microgeneration resource. This power source may be in the form of a small wind farm, fuel cells, small-scale hydro-electric systems, heat pumps, or more commonly rooftop photovoltaic cells. Energy harvesting devices require control especially in cases where the energy generated is in excess of system capabilities either in terms of power storage or supplying the load profile at any given time. Furthermore, the charging rate of the storage device is directly proportional to the amount of energy harvested.

4.2.2 The Storage Device

Central to the control system is the home energy storage device. This home energy storage device is comprised of a battery bank that may be made of lead acid, lithium ion, or vanadium redox batteries in series and parallel. The lifetime of the battery depends on thermal effects and battery degradation with respect to time. For most battery banks remaining energy capacity, lifetime, and efficiency are directly related to the operating temperature, the depth of discharge, the charging rate, and the number of charge/discharge cycles. To maximize the lifetime of the battery, it becomes necessary to monitor and control the temperature and charging rate as both effect the material properties of the electrodes which develop cracks over time. To make distributed energy resources more popular in the residential sector, the amount of money saved from switching to renewables must offset the initial installation and maintenance costs of the system as a whole.

4.2.3 Load Profile

The consumer interacts with the system through aspects of their daily life and habitual energy usage. As we saw in the previous chapter, a resident load profile is informed by daily activities. On average, the daily activities of the neighborhood contribute to a local load profile which may be designated as low or high demand at any given time. It becomes necessary for the system to anticipate changes in load profile with the course of the day, available harvestable energy, and future demand. While in this section the load takes a more generalized role, the work established thus far allows the system to be analyzed at a smaller scale though not the topic of this section directly.

4.2.4 Grid

The utility, or grid, determines the pricing available to the resident at a particular time of day (TOU) or due to specific market demands (in the case of dynamic pricing). Depending on the amount of available stored power, charge rate control, or future harvestable power, the home energy management system may choose to draw power from the power grid. The cost of utility supplied power is a function of time with power rates low during off-peak hours and high during peak hours.

4.3 Harvesting Power: irradiance as a function of cloud cover

In this section we seek to build a stochastic weather model to find the global irradiance for a specific time of day and a particular cloud cover percentage. We download

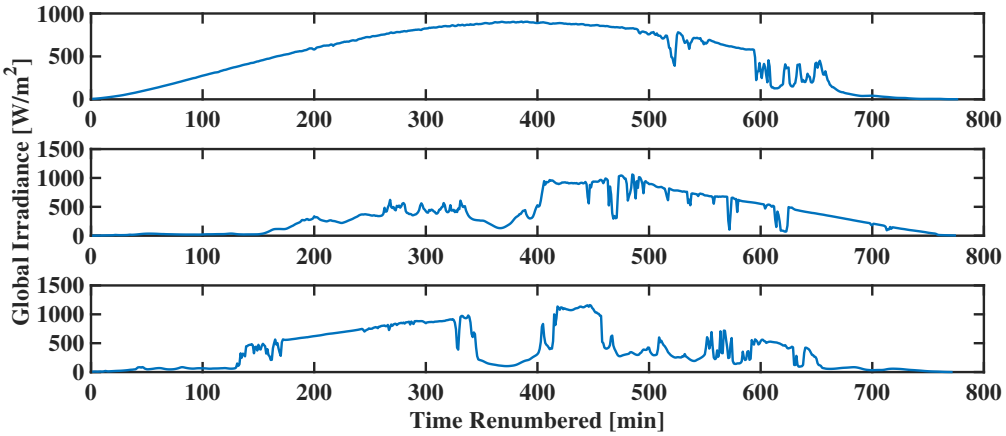

Figure 4.2: Daytime global irradiance as a function of time for Golden, Colorado for September 1, 2, 3 2016. The time axis has been renumbered to align the days with respect to the irradiance. Daylight for September 1st, 2nd, and 3rd begin at 5:32am, 5:33am, and 5:34am respectively.

datasets from the National Renewable Energy Solar Radiation Research Laboratory baseline measurement system in Golden, Colorado. We choose this specific location due to the variability in cloud cover and weather patterns in contrast to locations with stable and consistent weather patterns. This allows us to take into account a wider range of possible cloud cover states and their effects on the global irradiance. We seek to analyze the data for a specific month of the year over ten years in an unsupervised manner. In previous work, cloud cover data is used to directly calculate the global irradiance incident on a solar panel based on astronomical and atmospherical constants dependent on the location, time of day, season, and earth's tilt angle (17). To simplify and generalize the model, we ignore these parameters and analyze the dataset directly at the ground level.

The month chosen for our study is the month of September, a time of year where the amount of daylight hours are relatively equal to the amount of evening hours in the northern hemisphere. The dataset is then divided into daylight hours for each day of the month. Daylight hours result in positive harvestable irradiance measurements, while evening hours result in negative un-harvestable irradiance from below the panel.

To further simplify data analysis we note that the variation in irradiance is negligible in adjacent days. Taking this into account we group the individual days of the month of September into groups of three days which show similar seasonal behavior. Since we would like to compare this model with readily available information we take into account the common meteorological forecasts given for cloud cover. In most weather news outlets the cloudiness of the day is assessed as "clear", "sparse clouds", "partly cloudy", "cloudy," and "overcast." By taking this into account, we bin the cloud cover data into four sets corresponding to cloud cover between $0-25\%$, $26-50\%$, $51-75\%$, and $76-100\%$ each corresponding cloud cover associated with "sparse clouds," "partly cloudy," "cloudy," and "overcast." This way we can examine ten datasets each of three adjacent days in the month of September for a particular cloud cover state over the course of ten years. Keep in mind that this breaks up the time series data of global irradiance into varying segments associated with a particular cloud cover. Given that we are interested in transitions between irradiance states, single datapoints in a sequence associated with a cloud cover state are not considered as they do not transition to another state in a time sequence. In Figure 4.3 we plot the global irradiance as a function of cloud cover for the first set of days in September at the noon hour where the irradiance is expected to be the highest. The color of each datapoint represents a set of cloud cover and irradiance measurements for a particular year. Since we are doing an unsupervised learning analysis, we do not include the Figure legend.

While the actual global horizontal irradiance itself follows a Gaussian relationship with some noise as shown in Figure 4.2, to capture the variability of cloud cover we break up the irradiance into hourly time segments and model the system using an inhomogeneous in time discrete Markov model for the global irradiance as a function of cloud cover. The model constructed is inhomogeneous in time to alleviate astronomical and atmospherical considerations in the calculation of irradiance. With-

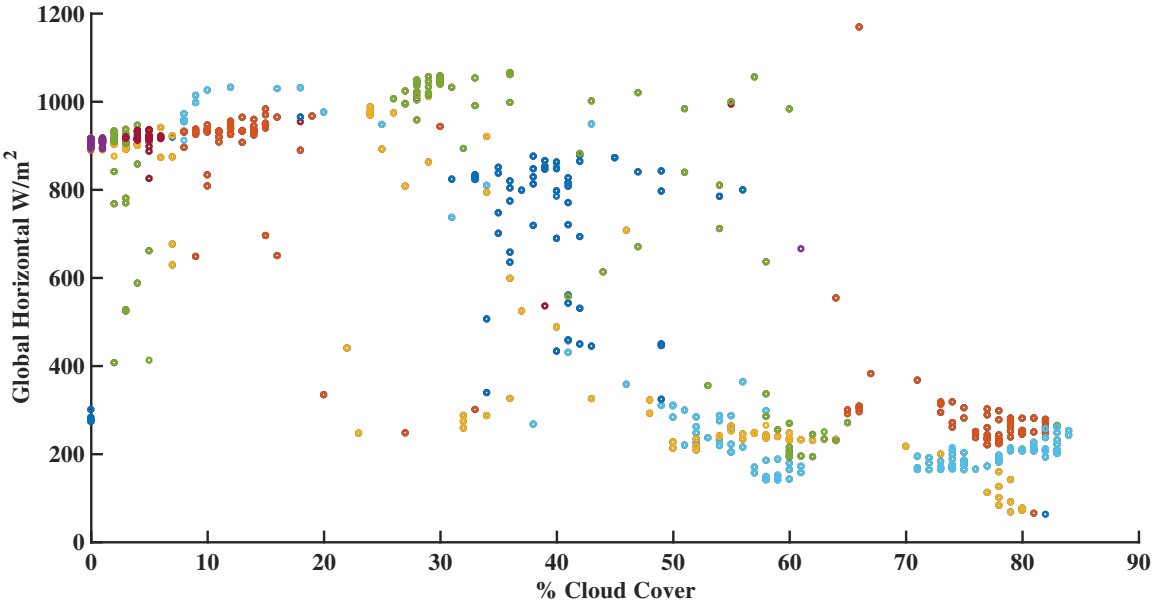

Figure 4.3: Noontime global irradiance as a function of cloud cover for Golden, Colorado from 2005-2015. The color of each datapoint corresponds to a particular unlabeled year. Unsupervised learning techniques are used in the analysis of this data.

out a Markov model, irradiance would have to be deterministically calculated using environmental information that may not be readily available without specific instrumentation. In this model, the current state of the irradiance is dependent only on the previous state. Since the model is inhomogeneous in time we calculate the Markov transition matrix for each hour using the hourly datasets of three day groupings as aforementioned. To reduce the number of states in the global irradiance data, we bin the global irradiance for all hours and sets of three day groupings to a finite number of states across all the datasets for each hour and cloud cover. The data must be binned across all irradiance data for all times of day to ensure that the transition matrices between each hourly time slice contain the same number of states and therefore matrix dimensions are constant. Reducing the number of states does not affect the model negatively since the purpose of the weather model is to infer the photovoltaic cell output which depends on the physical properties of the semiconductor material beyond a specific threshold voltage.

The Markov transition matrix g can be estimated element-wise $\hat{g}_{ij}$ using the global horizontal irradiance data with a finite state space $\mathcal{S}_g$ for a given cloud cover C_T for the hour T by calculating the frequency f of transitions from a starting state i to a particular state j over the total number of transitions from state i to states in the state space.

$$\hat{g}_{ij|C,T} = \frac{f_{ij}}{\sum_{k=0}^{\mathcal{S}_g} f_{ik}} \tag{4.1}$$

$$P(G_{t+1}{=}g_j|G_t{=}g_i, C_T, T) = g_{ij|C_T,H} = \begin{bmatrix} \hat{g}_{00} & \hat{g}_{01} & \cdots & \hat{g}_{0\,\max(\mathcal{S}_g)} \\ \hat{g}_{10} & \hat{g}_{11} & \cdots & \hat{g}_{1\,\max(\mathcal{S}_g)} \\ \vdots & \vdots & \ddots & \vdots \\ \hat{g}_{\max(\mathcal{S}_g)0} & \hat{g}_{\max(\mathcal{S}_g)1} & \cdots & \hat{g}_{\max(\mathcal{S}_g)\,\max(\mathcal{S}_g)} \end{bmatrix} \tag{4.2}$$

4.4 Photovoltaic power generation

Since we take into account the local weather forecasts and model irradiance as a random function dependent upon local cloud cover and time of day as a Markov chain, we may calculate the approximate current and power generated for a single photovoltaic panel based on the irradiance and manufacturer specifications. Since the photovoltaic cell is comprised of a p-type and n-type semiconductor junction, the photovoltaic panel is characterized by its current-voltage or IV relationship illustrated

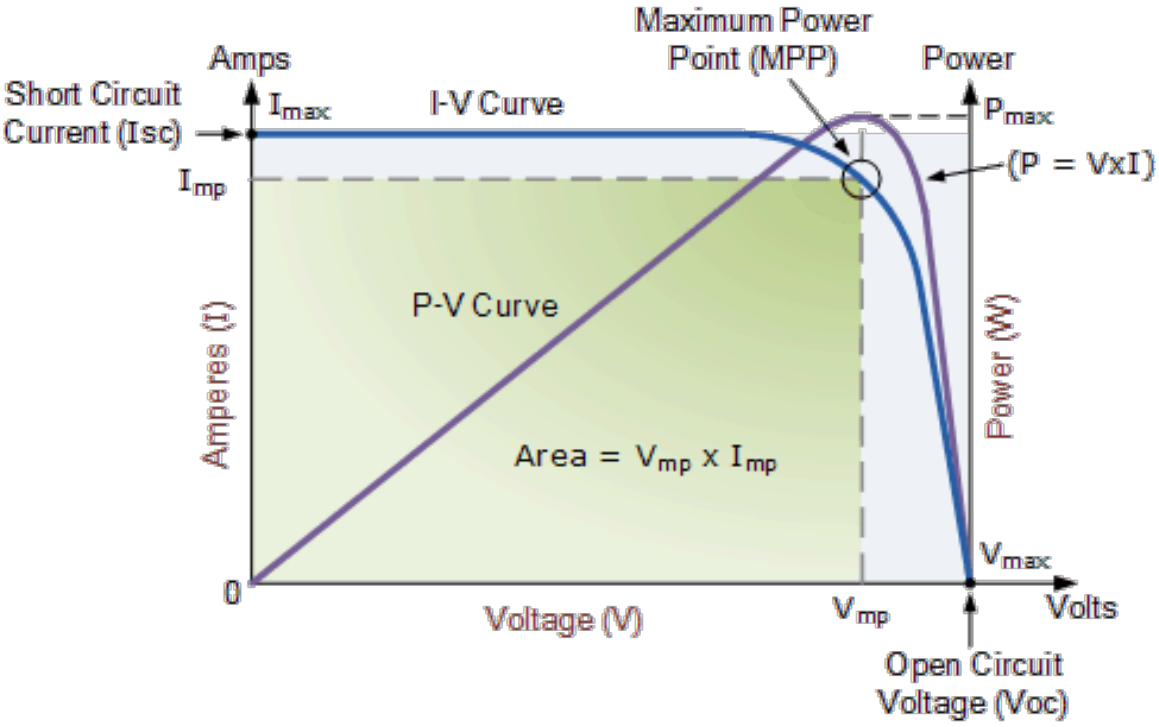

Figure 4.4: Photovoltaic IV characteristics (33).

in Figure 4.4 . In other words,

$$i_{out} \approx i_{sc}(.001 * g_t) - i_o[exp(\frac{qv}{nkT_k}) - 1] \tag{4.3}$$

$$p = i_{out} * v_{mppt} \tag{4.4}$$

where i_{sc}, v_{mppt}, and i_o are current and voltage parameters available in the photovoltaic panel specifications and q, v, n, k, and T_k are physical constants.

The power p output by the photovoltaic panel is assumed to operate at the maximum power point voltage. To ensure maximum power transfer from the solar panel to the energy storage device, we assume maximum power point tracking electronics are employed to maintain a constant voltage v_{mppt}. Since the electronics interface with the photovoltaics and home energy storage some loss in power is expected. Available maximum power point tracking devices are reported to have an efficiency between

94-97%. We can therefore assume that the power input to the battery at any given time can be calculated as

$$p_{in} \approx \eta_{mppt}(i_{sc}(.001 * g_t) - i_o[exp(\frac{qv_{mppt}}{nkT_k}) - 1]) \cdot v_{mppt} \tag{4.5}$$

The input power, however is calculated over a given hour. To get the rate of power charge into the battery, we divide by sixty to calculate an input power rate, or energy quanta over a minute since the irradiance for a given cloud cover is subject to changes at a higher resolution than over the hour. We express the value of the harvested quanta as the random variable H:

$$H_t = h_i = p_{in}/\Delta T \tag{4.6}$$

$$H = \{H_t{=}h_i, i, t \in \mathbb{N}^+\} \tag{4.7}$$

where $H_t = h_i$ represents the harvested input energy quanta at discrete time t for a state space $\mathcal{S}_{\mathcal{H}}$. p_{in} represents the calculated input power from the energy generating device, and ΔT is the period of time we use to scale quanta as a rate. Since p_{in} is driven by the incident global horizontal irradiance G characterized by the transition matrix $P(G_{t+1}|G_t, C_T, T)$. We can translate G to H as the scaled transition matrix $P(H_{t+1}|H_t, C_T, T)$ allowing us to relate solar irradiance in units of harvested energy quanta available to the energy storage battery.

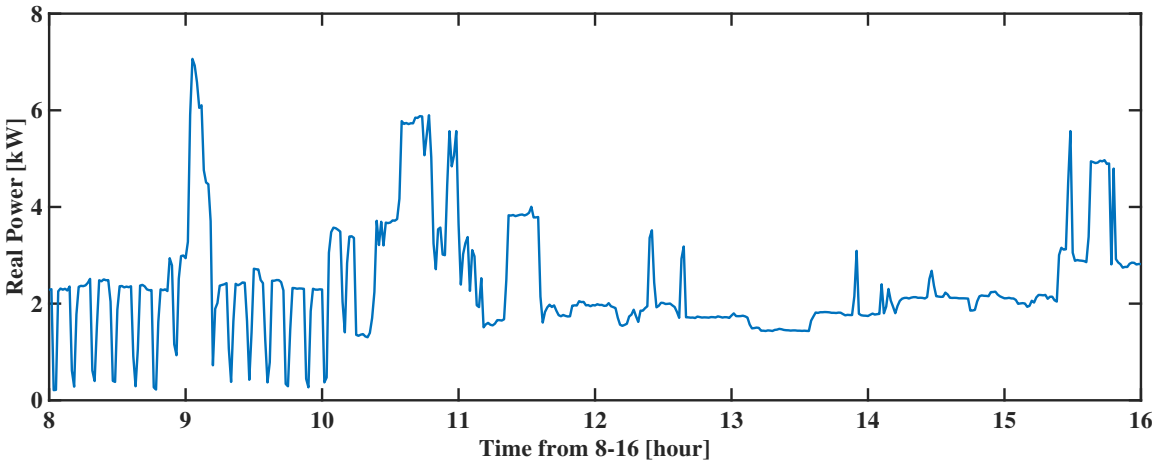

Figure 4.5: Consumption load profile for an individual household taken from the UCI Machine Learning Repository.

4.5 Consumption Load Profile

The consumption load profile, shown in Figure 4.5, for a given household is estimated by analyzing individual household load profile data available through the UCI Machine Learning Repository (34).

As in Section 4.3, the a sequence of power values are discretized in state space comparable to the state space of the energy harvesting block. We can directly calculate the energy quanta required by the load L by scaling the power to output energy quanta as $p_{load}/\Delta T$. Since L is dependent on resident power usage susceptible to random variations throughout the day, we express L as a Markov model and calculate the transition matrix by counting the transitions of a starting state to an individual state averaged over all transitions initiated from the starting state. To simplify our unified stochastic model of the residence we assume that the load profile is homogeneous in time. Therefore,

$$\hat{l}_{ij} = \frac{f_{ij}}{\sum_{k=0}^{\mathcal{S}_l} f_{ik}} \tag{4.8}$$

$$P(L_{t+1}{=}j|L_t{=}i){=}l_{ij}{=}\begin{bmatrix} \hat{l}_{00} & \hat{l}_{01} & \cdots & \hat{l}_{0\,\max(\mathcal{S}_l)} \\ \hat{l}_{10} & \hat{l}_{11} & \cdots & \hat{l}_{1\,\max(\mathcal{S}_l)} \\ \vdots & \vdots & \ddots & \vdots \\ \hat{l}_{\max(\mathcal{S}_l)0} & \hat{l}_{\max(\mathcal{S}_l)1} & \cdots & \hat{l}_{\max(\mathcal{S}_l)\,\max(\mathcal{S}_l)} \end{bmatrix} \tag{4.9}$$

for a discrete time increment t. Alternatively, we can express the Markov chain L as $L = \{L_t = l_i, t, i \in \mathbb{N}^+\}$ for l_i in a discrete state space $\mathcal{S}_\mathcal{L}$.

4.6 Energy Storage Unit

The resident distributed energy resource requires a means of storage in order to take full advantage of the energy harvested during the daytime. In order to do so, we incorporate a home battery bank in the resident energy system model. In practice, the battery bank consists of several batteries in order to increase storage capacity based on energy availability, battery type, and environmental conditions. Several battery types exist on the market such as lead acid, lithium ion, and redox flow for residential battery banks. Differences between the battery types are dependent on the cost, capacity, power ratings, depth of discharge, round trip efficiency, battery lifetime, and manufacturing (35). Depth of discharge (DoD) in particular directly affects the battery lifetime and is dependent on the capacity of the battery. In other words, the chemical composition of the storage unit requires the presence of charge. If the maximum capacity of the battery is being used, the lifetime of the device will decrease over time. Manufacturer suggested DoDs below the maximum capacity are provided for optimal device performance. Round trip efficiency, on the other hand, is the amount of electricity that can be provided by the battery given the input elec-

tricity from the connected power generator such as the photovoltaic panel. In other words, it is the amount of usable energy you can extract given the amount of energy stored. Typically, the efficiency is less than one hundred percent, or maximum energy harvested, indicating some losses are incurred from the input power. This loss needs to be factored in when designing a battery bank necessary to sustain a consumption profile off-grid given the amount of power generation from the photovoltaic energy source. The lifetime of the battery, as aforementioned, is dependent on the battery capacity and the depth of discharge. The amount of charge extracted or inserted to the battery by the load or photovoltaic panel affects the charge and discharge rate or cycling of the battery. Most battery manufacturers provide warranties covering a certain number of cycles per year given that the battery is operated at optimal conditions and recommended depth of discharge. This is due to the charge capacity of the battery which decreases with usage. Since most photovoltaic panels have lifetimes of twenty-five to thirty years, at least one battery bank replacement is expected. To maximize the lifetime of the battery it becomes necessary to control the DoD. The physical properties of the battery also control the extent of charging and discharging as the state of charge varies between low and maximal charge levels (18). The charge discharge rate of the battery varies as a function of the state of charge. A battery charged at half capacity has a higher charge discharge rate than a battery at zero charge. When the battery is fully discharged which is not recommended, the battery charge rate is slow. When the battery is fully charged, or at maximum capacity, the battery is saturated and can no longer accept incoming charge. While not considered in this study, temperature may also be detrimental to energy storage performance. Temperatures below 30 deg F increase the maximum power point voltage that the battery requires for low loss power transmission. Temperatures that exceed 90 deg F result in charge reduction due to battery overheating thereby requiring residents to set up battery banks in temperature controlled environments resulting in infrastructural

and cost overhead (35).

We simplify modeling the battery bank by assuming that the voltage across all batteries is constant and that the batteries are all of the same type in terms of manufacturing. We also assume that the battery banks are in a controlled temperature environment allowing the storage device to operate in ideal conditions exclusive of the ambient temperature outside the home. Furthermore, we model the battery bank as a single battery with a specific amount of discrete quanta level for continuity with respect to the rest of the unified model in terms of Markov chain characteristics. Each quanta corresponds to a specific charge in the battery and can be described at any time as the superposition of the current battery charge, the proportion of charge drawn from the battery due to the residential load profile, and the input power quanta supplied from the energy harvesting device. Explicitly,

$$Q_{t+1} = Q_t(1 - \alpha) + H_t \tag{4.10}$$

where Q_{t+1} represents the energy quanta at the next time trial given that the current value of the energy quanta charge state minus the proportion α of energy quanta drawn from the load and the energy harvest input H_t in unit quanta.

4.7 Grid Supply

To take into account modern home energy systems, the residential load profile may draw energy from the battery, the grid, or a combination of both. In other words, the system may choose to take a certain proportion of energy from the energy storage device and the remaining portion from the grid. The adjusted load seen by the grid energy metering device is the difference between the actual load profile and the

proportion of energy drawn from the energy storage device. In other words,

$$L_{grid_t} = L_t - \alpha Q_t \tag{4.11}$$

where L_{grid_t} represents the load from the perspective of the load at discrete time t, L_t represents the actual resident load, and α represents the proportion of energy Q_t taken from the battery.

While we do not take into account in detail the power electronics associated with inverting the battery power from DC to AC to support the load, we remark that the model can be adapted by approximating the inverter as an efficiency term. Indeed in the case study presented we scale the battery supplied power with an efficiency term.

4.8 Control

The equation 4.10, while descriptive of the system when connected to the battery, requires that the battery have an adequate amount of existing charge or input energy harvested H in order to meet the proportion of charge required by the load demand L at any given time. In off-grid conditions, loads that exceed both Q and H may place the residence in danger of power outage. Therefore, the approach to control in this work enables the energy management system to optimize the proportion of energy drawn from the storage unit while still connected to the grid. In other words, the energy management system has the flexibility to draw power from the battery when adequate supply, load, and irradiance conditions allow for off-grid status while still maintaining connection to the grid should the system require it. By maintaining connection to the existing grid power drawn from the battery may be scheduled based on grid conditions and demand response programs to minimize time of use pricing

and peaks in community demand.

The system must also take into account the energy storage device. The battery itself has physical limitations with respect to its lifetime and the amount of stresses it can incur upon usage over time. Both of these concerns are addressed in a control mechanism whereby the residential energy system can control the amount of energy drawn from the grid and the energy storage device to supply the load as well as the rate of charge from the energy harvester to the storage unit.

4.8.1 Load to Battery and Grid Connection

In Figure 4.1, the energy management system may choose to draw a specific amount of power from the battery and the grid in a manner similar to a valve. In other words, the amount of energy taken from the grid and the battery can be tailored to take more power from the grid during off-peak hours to take advantage of pricing and allow the battery to charge. Alternatively, a greater proportion of energy may be drawn from the energy storage unit during ideal battery operating conditions or at times when peak demand causes electricity pricing to fall out of the budget of the resident.

As aforementioned, homes would require interfacing power electronics such as inverters to convert direct current to alternating current, correct for power factor, and feed from the energy harvester to the grid at any given time. Since we model the contributing elements of the home energy system as Markov chains to be used in a Markov decision process for control optimization, the system is subject to the curse of dimensionality–or a large number of states. Having a large number of states is undesirable as it requires more processor power which may not be realistic for a simple at home system to be used in a similar capacity to that of a thermostat. We therefore, simplify the process by introducing control in terms of the proportion of energy drawn

from the energy storage unit to the load $\alpha = \{\alpha_n, n \in \mathbb{N}^+\}$, where $0 \leq \alpha_n \leq 1$. For example, $\alpha = \{0, 1/4, 1/2, 3/4, 1\}$, representing the capacity of energy taken from the current charge of the battery. In other words, the increments of α behave similar to a discrete cumulative distribution function over a probability distribution depending on the characterization of the quanta Q. In the example presented as well as the case study that follows, the battery quanta are assumed to be equal and uniformly distributed from the minimum capacity to the maximum capacity of the battery. Therefore, the battery charge quanta that can be supplied to the load at any given time is $Q_{supp_t} = Q_t(1 - \alpha_n)$, where we assume that the battery is drawn at the end of the interval. $\alpha_n = 0$ represents the condition that no current battery energy is drawn from the battery to supply the load and $\alpha_n = 1$ represents the condition that all current battery energy is drawn.

It is important to note that the maximum quanta of energy is described by the maximum capacity of the battery bank can supply based on its power and charge rating. The case where $\alpha = 1$ would result in full discharge of the current battery charge in the next time slice. Full discharge conditions fall outside manufacturer suggested settings. To tailor the system to meet manufacturer settings it is worth noting that the model minimum battery quanta Q_{min} can be set to a value greater than the zero charge level of the battery. Similarly, Q_{max}, or the maximum amount of battery charge can be tailored to less that one hundred percent capacity to fall under warranty settings.

4.8.2 Battery to Harvesting Unit Connection

A second means of control is presented at the battery to the energy harvesting stage of the system which includes the photovoltaic panels and the maximum power point

tracking electronics as described in Section 4.4. A switch f_n connects the the residential load to the grid or to the battery. The switch $f_n =\in \{0, 1\}$ where $f_n = 0$ is the condition with which the battery is disconnected from the harvesting unit and $f_n = 1$ is the condition with which the battery is connected to the harvesting unit. This second level of control is chosen with respect to the battery charge and discharge. Charge/discharge of the battery has a direct effect on the energy capacity, lifetime, and efficiency of the battery. With increased battery use, the battery itself undergoes degradation. The reason for the degradation is a change in volume with respect to the cell electrodes that comprise the battery. Over time and usage the volume change causes microscopic fissures in battery electrode material which results in an increase in battery cell internal resistance, reduction in electrode contact, and overall battery capacity fading (36). The degradation of batteries is so common that the electric automotive industry associates the end of battery lifetime as a state where the current maximum capacity of the battery is eighty percent of the original capacity at time of purchase (36). The equation describing the state of charge changes with respect to the configuration of the switches connecting the system components at any given time. In other words, if the battery to energy harvesting stage switch is off, the battery is disconnected from the energy harvester. Such a condition may be ideal under conditions of battery saturation or to control the depth of charging in the battery at a given time.

4.8.3 Overall System Dynamics

Following the introduction of two degrees of control, α_n and f_n, over the allocation of energy from the grid, battery and the photovoltaic panel of the residence, we may reformulate the system dynamics in terms of the deterministic battery quanta relationship introduced in Equation 4.10 as well as the operational constraints of the

physical battery itself as suggested in 4.8.2. We express the overall system as the following:

$$Q_{t+1} = \min(\max(Q_t(1-\alpha_n) + f_n \cdot H_t, Q_{min}), Q_{max}) \tag{4.12}$$

$$H = \{H_t{=}h_i, i, t \in \mathbb{N}^+\}, \qquad \text{where } h_i \in \mathcal{S}_{\mathcal{H}} \tag{4.13}$$

$$L = \{L_t{=}l_j, j, t \in \mathbb{N}^+\}, \qquad \text{where } l_j \in \mathcal{S}_{\mathcal{L}} \tag{4.14}$$

$$f_n \in \{0, 1\} \tag{4.15}$$

$$0 \leq \alpha_n \leq 1, \tag{4.16}$$

where Q_{min} and Q_{max} ensure that the charging and discharging of energy quanta remain within the operating parameters of the battery.

4.9 Control Optimization

We optimize the control of proportion α_n and switch f_n by formulating the system as a Markov decision process described by system equations 4.12 and by constructing a cost function for use in the value function iteration described in Chapter 2. We construct a cost function as a tradeoff relationship between the cost of using the power grid and the cost of using battery. The cost of using the power grid can be described by the time of use (TOU) power rate as well as the residential load profile L_t at time

t. The cost of using the power grid given the electric power rate $e_{TOU(t)}$

$$C_g = e_{TOU(t)} \cdot L_{grid_t} \tag{4.17}$$

$$C_g = e_{TOU(t)} \cdot (L_t - \alpha_n Q_t), \text{ where } 0 \leq \alpha_n \leq 1 \tag{4.18}$$

$$\tag{4.19}$$

while the cost of taking power from the battery as defined in (18) can be approximated as:

$$C_b = \frac{Q_t}{Q_{max}} - \eta, \text{ where } 0 < \eta \leq 1 \tag{4.20}$$

where Q_{max} describes the maximum amount of charge quanta the battery is capable of storing and η is a charging efficiency parameter. For most batteries, η is .5, indicating that the battery charges most efficiently when $Q_t = 0.5 \cdot Q_{max}$. This is as expected because for Q_t close to Q_{max} results in slower charge efficiency as the battery has already reached a state of saturation. Conversely, for values of Q_t close to zero, the battery has little to no charge stored, the energy it takes to overcome the charging inertia of an empty battery is high so the state of charge efficiency is low. To construct a tradeoff between the physical costs of battery usage C_b and grid usage C_g requires that both values are normalized in a manner that can be superimposed into one defining cost function for use in the dynamic programming value iteration method for Markov decision processes. We observe that the value of C_b remains within a $[0, 1]$ whereas the value of C_g depends on the current TOU grid pricing. This observation, if unattended would result in a poor evaluation of the ideal Markov policy output of the value iteration function as the units and cost scales are mismatched. To alleviate this situation, we normalize C_g by the maximum L_{max} that the resident is capable of when all appliances in the home are drawing power. We rewrite the cost of the grid

as:

$$C_g = \frac{e_{TOU(t)} \cdot (L_t - \alpha_n Q_t)}{e_{TOU(t)} \cdot L_{max}} = \frac{L_t - \alpha_n Q_t}{L_{max}} \tag{4.21}$$

We can now formulate the overall system cost function using the tradeoff factor λ associated with the action parameters α_n and f_n as:

$$\sum C = \lambda \cdot C_g + (1 - \lambda) \cdot C_b \tag{4.22}$$

and thereby apply the value function iteration for Markov decision processes to arrive at an optimal policy or sequence of α_n, f_n actions.

4.10 Value Function Iteration

In this section we introduce the construction of the value function iteration parameters using the Markov system quantities thus defined as well as the introduction of hourly weather forecast in terms of cloud cover for the consumer residence location. Recall from Chapter 2, we define the value function for a Markov decision process using the Bellman equations. In other words, given:

$$\text{system state space} : S \tag{4.23}$$

$$\text{model} : P(s'|s, a) \tag{4.24}$$

$$\text{actions} : A(s) \tag{4.25}$$

$$\text{state-action state space} : SxA \tag{4.26}$$

$$\text{cost} : C(s, a) \tag{4.27}$$

$$\text{discount factor} : 0 \leq \gamma \leq 1 \tag{4.28}$$

we may derive an optimal policy $\Pi(s) \rightarrow a$ or a sequence of state-actions for the system for a time horizon of interest. The Bellman equations describing the generalized process are:

$$V(s) = \min_a (C(s,a) + \gamma \sum_{s'} P(s'|s,a) V(s')) \tag{4.29}$$

$$Q(s,a) = C(s,a) + \gamma \sum_{s'} P(s'|s,a) \min_a Q(s',a') \tag{4.30}$$

Recall from Chapter 2 the second Bellman equation is written in terms of what is known as a Q-state or state-action pair for a given time. Note that in the value function method the system recursively calculates the updated value using the previous value. In the Q-state packaging of the Bellman value iteration, the cost for all state action pairs for a given time step are calculated. The Q-state, state-action pair, that results in the minimum cost is thereby used in the iteration for the next state calculation. In terms of the established system parameters we may rewrite the residential energy Markov decision process as:

$$\text{state} : s{=}(H_t{=}h_i, Q_t{=}q_j, L_t{=}l_k) \tag{4.31}$$

$$\text{state space} : \mathcal{S}_{\mathcal{H}} \times \mathcal{S}_{\mathcal{Q}} \times \mathcal{S}_{\mathcal{L}} \tag{4.32}$$

$$\text{model} : P(H_{t+1}, Q_{t+1}, L_{t+1} | H_t, Q_t, L_t, \alpha_n, f_n) \tag{4.33}$$

$$\text{actions} : (\alpha_n, f_n) \tag{4.34}$$

$$\text{state-action} : s, a = (H_t{=}h_i, Q_t{=}q_j, L_t{=}l_k), (f_n, \alpha_n) \tag{4.35}$$

$$\text{state-action space} : \mathcal{S}_{\mathcal{H}} \times \mathcal{S}_{\mathcal{Q}} \times \mathcal{S}_{\mathcal{L}} \times \mathcal{S}_{\alpha_n} \times \mathcal{S}_{f_n} \tag{4.36}$$

$$\text{cost} : C(s,a){=}\lambda \cdot C_g((H_t, Q_t, L_t), (\alpha_n, f_n)) \tag{4.37}$$

$$+ (1-\lambda) \cdot C_b((H_t, Q_t), (\alpha_n, f_n)) \tag{4.38}$$

$$\text{discount factor} : 0 \leq \gamma \leq 1 \tag{4.39}$$

we may derive an optimal policy $\Pi(s) \rightarrow a$ or a sequence of state-actions for the system for a time horizon of interest. The Bellman equations describing the generalized process are:

$$V(h,q,l) = \min_{\alpha_n, f_n}(\lambda C_g((h,q,l),(\alpha_n,f_n)) \\ +(1-\lambda)C_b((h,q,l),(\alpha_n,f_n)))+\gamma \sum_{h',q',l'} P(h',q',l'|h,q,l,(f_n,\alpha_n))V(h',q',l')) \tag{4.40}$$

$$Q(h,q,l,(\alpha_n,f_n)) = C(h,q,l,(\alpha_n,f_n))+ \\ \gamma \sum_{h',q',l'} P(h',q',l'|h',q',l',(\alpha_n,f_n)) \min_{\alpha_n,f_n} Q(h',q',l',(\alpha_n',f_n')) \tag{4.41}$$

4.11 Controlling Battery Degradation

During each battery charge and discharge cycle microscopic structural damage occurs within the material. This damage occurs over time as the battery is used. Similar fatigue effects are well studied in materials science for use in construction of bridges and marine structures which are subject to variations in loading as well as temperature. For narrow-band Gaussian processes, the cycles are well defined however for more general stress information cycle counting methods are useful. In time domain, fatigue analysis uses the information provided by local maxima and local minima in stress data. This allows the stress ranges to be identified and grouped using cycle counting methods. Various cycle counting methods exist for this purpose such as peak counting, range counting, level-crossing counting, and rain flow counting. ASTM E

1049-85 establishes the rain flow counting method as a standard suitable for fatigue damage (37).

4.11.1 Rain flow counting method

The procedure for using the rain flow method manually is to observe the time series stress signal with the time axis drawn vertically downward. Then lines connecting peaks and valleys form a set of "pagoda roofs" as outlined by Matsuishi and Endo (38). The rules of the rain flow counting method are as follows:

- Begin at the first point in time at the inside of every peak and valley.
- Rain flow, if initiated from a peak drops down until it reaches an opposite peak which is more positive (or more negative in the case of a valley) than from the peak where the flow started.
- Rain flow stops when it meets flow from a roof above it.
- Rain flow must terminate at the end of a time series.
- The horizontal length of each flow between paths is counted as a half cycle with the length or amplitude as the stress range for the path.

More formally, the cyclic stress can be found by

$$\sigma_{ampl} = \frac{\sigma_{\max} - \sigma_{\min}}{2} \tag{4.42}$$

where $\sigma_{\max}$ and $\sigma_{\min}$ correspond to a peak or valley and *ampl* corresponds to a particular path of interest. Following the calculation of stress ranges for each individual path defining a half cycle (from a peak to a valley or vice versa), the paths can be

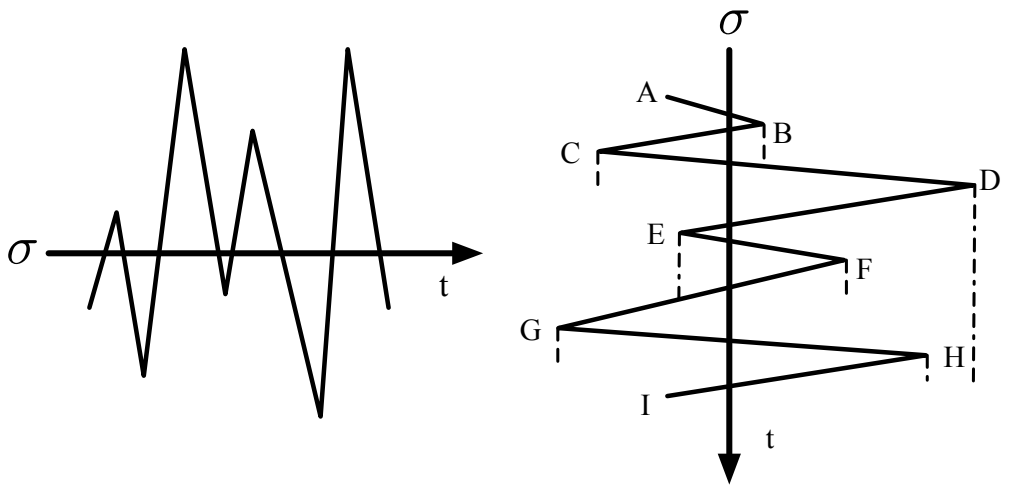

Figure 4.6: Rain flow counting method estimates number of cycles for each stress range by measuring the amplitude of stress for a given path. The paths in this example are AB, BC, CD, DG, EF, GH, and HI.

grouped according to the range of σ and the number of cycles n_g for a each group g which is simply the sum of the half cycles associated with each group of similar cycle. The damage for any particular group g of paths of equal stress range σ can be assessed by examining the material's characteristic Wöhler/S-N curve of cyclic stress. This curve is a bi-logarithmic graph which represents how well a material can withstand stress cycles. In other words it is characterized by

$$\log(\sigma_{ampl}) = \log(\sigma_{fail}) - m\log(N), \tag{4.43}$$

where σ_{fail} is the stress at static failure (also known as maximum yield strength) and N is the number of cycles. The maximum number of cycles can be calculated by manipulating Equation 4.43, to:

$$N_{max} = (\frac{\sigma_{fail}}{\sigma_{ampl}})^{\frac{1}{m}} \tag{4.44}$$

where m represents the slope of the σ_{ampl} vs N curve, or Wöhler curve. Typically, the S-N, or Wöhler curve of cyclic stress against the number of cycles to failure for a specific material. Most often, thee materials are available for construction materials such as steel, iron, and aluminum. Battery material Wöhler curves are difficult to find and must be estimated based on other fatigue parameters. In this work we use the methods introduced in (39) to approximate the S-N parameters for fatigue life calculation for the battery given the battery charge/discharge history. In the case of the lithium ion battery we recognize that the mechanical electrode damage must be evaluated in terms of the stress based on the depth of discharge and state of charge. The fatigue life calculation is necessary in the benchmarking of control and its effectiveness in extending the battery life while minimizing the cost of taking power from the grid directly as well as minimizing overall battery damage.

4.11.2 Cumulative Material Damage

The Palmgren-Miner(40) cumulative fatigue damage D is calculated as

$$D = \sum_{i=1}^{k} \frac{n_i(\sigma_{ampl\ i})}{N_{max\ i}} \tag{4.45}$$

$$D = \sum_{i=1}^{k} (\frac{\sigma_{ampl\ i}}{\sigma_{fail}})^{\frac{1}{m}} n_i(\sigma_{ampl\ i}) \tag{4.46}$$

$$\frac{D}{Cycle} = (\frac{\sigma_{ampl}}{\sigma_{fail}})^{\frac{1}{m}} \tag{4.47}$$

$$\frac{D}{Cycle} \propto \frac{Cap_{loss}^{T}(\%)}{Cycle} \tag{4.48}$$

$$\frac{Cap_{loss}^{T}(\%)}{Cycle} = \frac{Cap_{loss}^{CAL}(\%)}{Cycle} + \frac{Cap_{loss}^{CYC}(\%)}{Cycle} \tag{4.49}$$

$$\frac{Cap_{loss}^{T}(\%)}{Cycle} \approx \frac{Cap_{loss}^{CYC}(\%)}{Cycle} \tag{4.50}$$

$$= A_1(\frac{\sigma_{ampl}}{\sigma_{fail}})^{\frac{1}{m}} \tag{4.51}$$

where A_1 is the capacity loss percentage factor. Using the values fitted in the study presented in (39) we use the following values for each constant:

A_1 [%/cycle]	0.04519
m	0.4926
σ_{fail} [MPa]	8

Therefore to calculate the accumulated damage we may write:

$$D = A_1(\frac{\sigma_{ampl}}{\sigma_{fail}})^{\frac{1}{m}} \cdot Cycle \tag{4.52}$$

4.12 Case Study

In this section we provide a case study demonstrating the optimization control of a residence in Golden, CO from September 1-3, 2016. Golden, CO was chosen as a location due to its variety and complexity of weather patterns and cloud cover. The month of September was chosen due to the daytime hours which roughly equal the amount of dark hours during the day. The models were built using historical weather and irradiance datasets available through the National Renewable Energy Laboratory from 2005-2015 after discretization and preprocessing the data. The load profile was also built using historical datasets provided by the University of California, Irvine Machine Learning Repository. Forecast information was web-scraped using the Beautiful Soup python package on weather channel information for up to nine hours beyond the present time.

The grid costs were based on the hourly rate advertised by the local utility which varied depending on the time of use and peak demand hours. However, in the end the cost was normalized thereby dependent proportionally on the difference of the

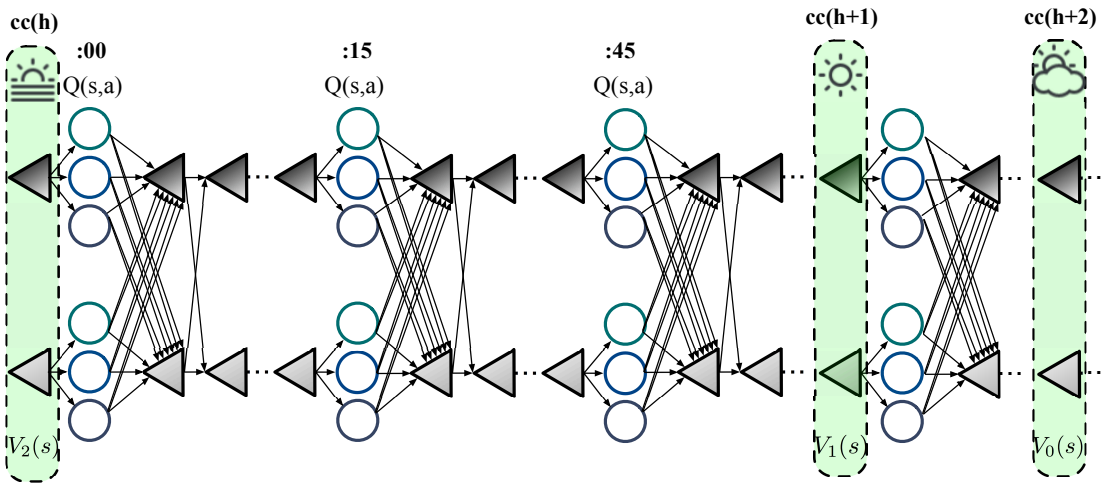

Figure 4.7: Generalized value function iteration tree over the course of the hourly forecast. Note that actions are only selected every fifteen minutes based on the forecast. The procedure is repeated as each hour of current cloud cover is read and the new forecasted data is assessed. For each triangle, or state that the state-action leads to, a subchain is initiated with respect to the irradiance, load profile, and the battery quanta state though not depicted.

current load and the drawn battery power with respect to the grid at a given time. Battery costs were determined using the operational physical equations presented in 4.11. The battery parameters used for this study are those for the lithium ion battery.

The value function was run over the forecast data starting four hours from the present time. Following the evaluation of the cumulative sum of the costs, the action associated with the minimum cost at the present time for the present cloud cover information was chosen. Actions were chosen every 15 minutes taking advantage of forecast data. The actions, once again are defined as the proportion of energy quanta drawn from the energy storage unit to support the load and the energy harvesting switch to the rechargeable battery. The simulation then ran for the present hour. Upon the start of the next hour, the value function again was evaluated starting four hours into the future using the forecasted data until the sunset and the system was no longer receiving radiant power to the energy harvesting device.

Simulations for the system Markov Decision Process were performed for $0 \leq \lambda \leq 1$ in increments of $\lambda = .05$. For one hundred sample functions of load and irradiance given cloud cover and hour, the battery charge and discharge profiles based on varying cost function was assessed in terms of aging. Simulation results show the predicted irradiance based on the cloud cover from the forecasted data as well as the inhomogenous in time Markov model built using historical data. The irradiance due to the binning algorithm to reduce states result in quantized outcomes that are apparent in the artifacts present in the irradiance profile H which show a similarity to the September 3rd Figure 4.2. September 3rd is analyzed and presented due to its variability with respect to cloud cover. The load profile model has been isolated to daylight hours associated with the averaged dataset and is labeled as L. Recall that the total cost in general was expressed as $C(s,a) = \lambda C_g(s,a) + (1-\lambda)C_b(s)$ where the cost was a function of both the current system state generalized as s and the action generalized as a. Recall C_g an C_b represented the grid and battery costs respectively. Results support improved system dynamics with energy management system implementation. We observe in Figure 4.8 that the charge discharge profile of Q is very much dependent on the cost parameter λ. In other words, when $\lambda = 0$, the system minimizes battery damage maintaining the ideal operating point of fifty percent of the total charge capacity. The system minimizes battery aging cost exclusively. Conversely when $\lambda = 1$, the system minimizes grid cost exclusively and draws from the battery quanta, or energy storage unit thereby resulting in greater deviations from the ideal operating point and more depth of discharge. In the case where $\lambda = 0.5$ both the grid cost and the battery aging cost are weighted equally. From varying the value of λ, it is clear that when optimization favors the battery completely the fluctuations in charge discharge cycles are flatter ($\lambda = 0$). When λ is tuned with some favoring towards the grid, when $0.5 < \lambda \leq 1$, the fluctuations from the ideal operating point increase as the battery is charged and discharged more readily as illustrated in Figure

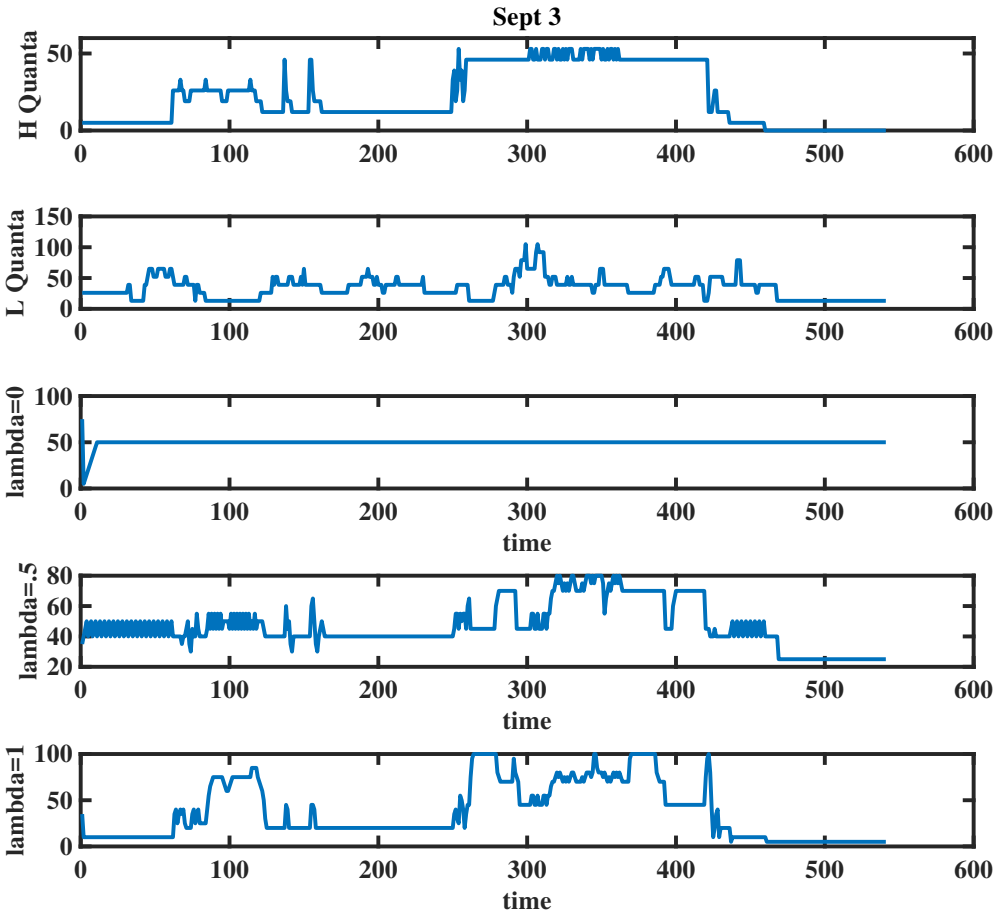

Figure 4.8: Simulation results for Q battery quanta charging profiles for cost parameter $\lambda = 0$, $\lambda = .5$, and $\lambda = 1$ for a sample function of H harvest quanta and L load quanta for September 3, 2016.

4.9.

Figure 4.10 presents the battery degradation or damage calculated after the charge discharge profiles of Q for each lambda value $0 \leq \lambda \leq 1$ of one hundred sample functions of irradiance H and load L data are generated. The turning points as outlined in the rainflow method of the charge profiles are then calculated. Upon rainflow analysis of the turning points using the physical parameters from (39)we observe that λ as defined in the optimization cost function is directly proportional to the battery aging

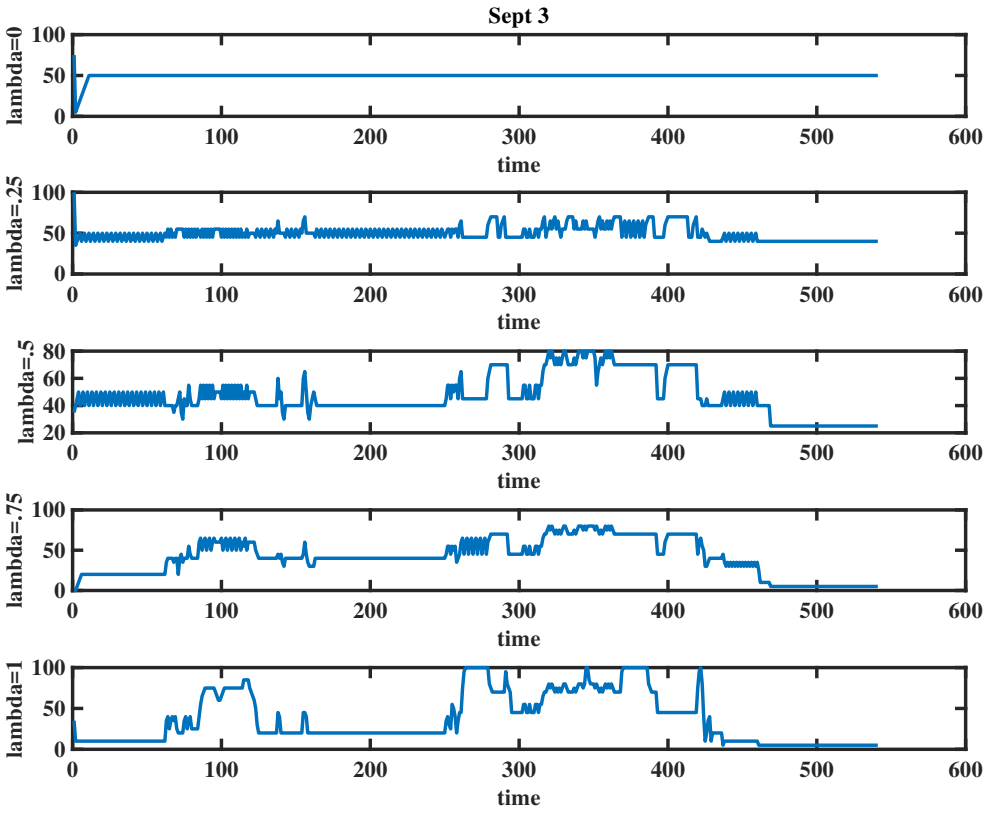

Figure 4.9: Battery quanta Q charge profiles for one sample function of H harvest quanta and L load quanta for September 3, 2016. λ values range from $0 \leq \lambda \leq 1$.

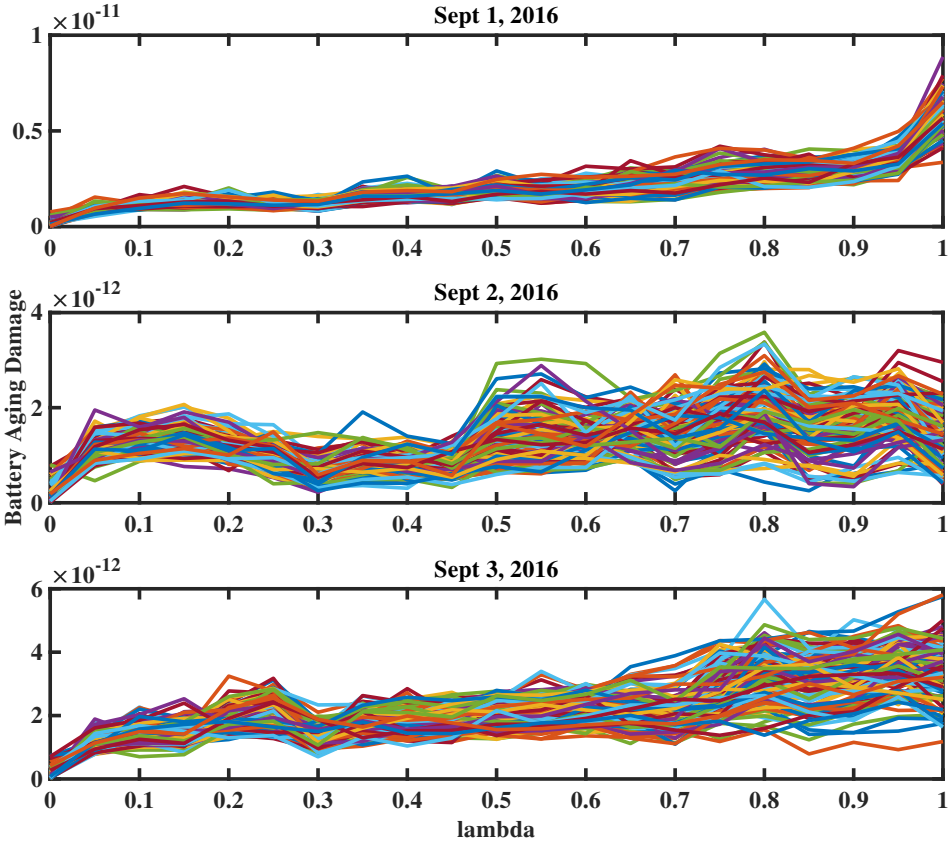

Figure 4.10: Battery aging degradation as a function of the cost parameter λ for one hundred sample functions of H irradiance quanta and L load quanta.

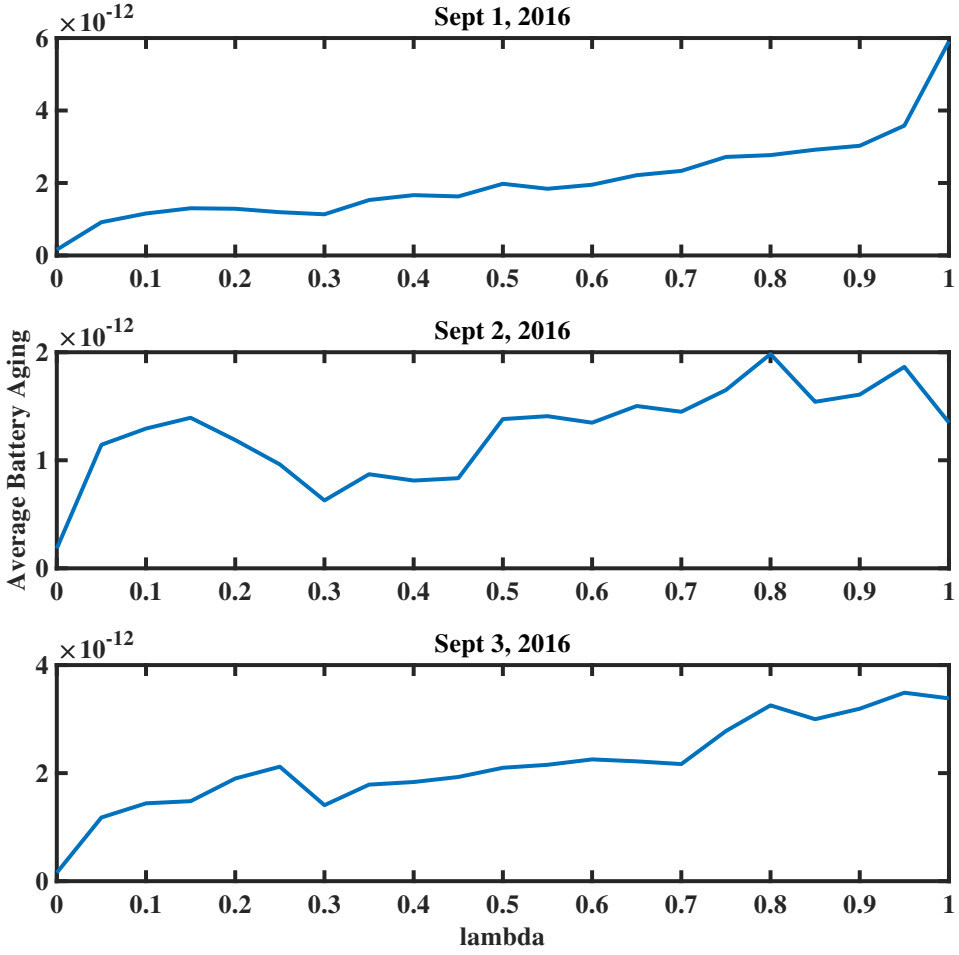

Figure 4.11: The averaged battery aging degradation over one hundred samples as a function of the cost parameter λ.

degradation. Averaged results over one hundred samples are presented in Figure 4.11. In other words as the cost parameter λ increases the weighting of the battery cost decreases resulting in greater battery degradation.

Chapter 5

Conclusion

In this paper we proposed an energy control framework driven by consumer behavior as an alternative to price driven systems. The EMS detected behavior according to pre-built reference models differing in activity sequence. Following model detection, the intelligent control agent assessed user appliance requests based the state estimate, a grid-informed consumption constraint, and a consumer convenience parameter. Results support that inclusion of human behavior as a driver for demand affects accurate consumption prediction which is necessary for EMS appliance scheduling. Consumer convenience constraints based on the current state estimate and the consumption constraint provided a means for the resident to control appliance activation delay. A case study demonstrated the effectiveness of the system as a whole. An additional control framework for residential distributed energy resources is also proposed. In this framework, the EMS agent schedules the charge and discharge of the energy storage unit in a residential microgeneration system consisting of an energy harvesting unit in the form of rooftop photovoltaic panels, a lithium ion battery bank, and the original consumer behavior driven load profile introduced in the first half of this work. Using historical datasets to build irradiance models which are inhomogeneous in time as a

function of cloud cover we are able to characterize the amount of energy harvested based on readily available weather forecast data without the use of expensive instrumentation. The forecast data, and the construction of the cyber-physical system as a Markov decision process, allows the control agent to assess the best possible action or long-term policy to reduce the overall cumulative cost to the residential consumer in terms of electric power rates as well as battery lifetime. Results support the control framework as an accurate means of controlling the material damage the battery may incur during its usage. The rain flow counting method for materials show a marked improvement in performance with respect to slow charge/discharge rates and overall cumulative battery damage.

Chapter 6

Future Work

Future work in this project can take many interesting directions. In the paper presented, we considered the control and appliance scheduling for the dishwasher. In reality, different heavy consumption long-term appliances may be considered in other case studies. For example, the HVAC, which we have included in our case study as a long-term activity dependent appliance, represents a major load that has been the target of discretionary utility programs within current demand response. In the study presented, we did not seek to control this particular appliance due to dependencies with respect to the external temperature and weather, but we did include it as an influential contribution to the aggregate load. Additionally, our residence case simulation study presented the EVSE as a load that is used simply to charge the car with a dependency on consumer occupancy via the detection of the activity *leave*. We did not consider using the car battery as a distributed energy resource (DER) in addition to the battery bank. We built upon the resident case study with the inclusion of energy resources such as energy storage systems and photovoltaic cells whose lifetimes depended on charge/discharge stress as well as cloud cover respectively. However, we did not take into account a control optimization system that connected the battery to

the grid via power electronic inverters to feed the harvested and stored energy back to the grid. Similarly, we did not take into account the case where the residence may take power both from the the grid and the battery. A natural extension of this work would be to control the ratio of power taken from the battery and/or the grid at any given time to reduce the overall cost of battery operation and utility power rates. In addition to further appliance case studies, alternative EMS frameworks may also be considered using different mathematical models for activity detection and appliance scheduling. Unfortunately, frameworks based on Markov models suffer from the curse of dimensionality. In other words, the amount of states with respect to individual users, behaviors, and appliance states quickly becomes intractable impacting the optimization process used to implement system control. Recall, in Section 3.4.1, we calculate the probability of exceeding a power grid defined threshold over a finite horizon corresponding to the cycle duration of a long-term appliance. The complexity of this process in terms of the number of operations required for calculation grows with the number of states where each time slot requires $O(S \times S)$ operations (41). Calculations are especially difficult when scaling the framework to a neighborhood or residential group level. Large state spaces correspond to lengthy estimation, slow convergence and high complexity of optimization. To scale up our model we must reduce the model or use alternative techniques. Alternatives such as graph signal processing approaches as presented in (42) may alleviate complexity issues. We leave a thorough evaluation of alternative techniques in the scenario described in this paper for future work. Finally incorporation of complementary work in non-intrusive load monitoring may inform better generalized appliance models. For example, (43) generalized appliance models from sub-metered appliance datasets of different makes and models of devices using supervised learning techniques followed by sampling to obtain averaged appliance instances depending on the appliance type. The general models were then used to disaggregate load curves from publicly available consump-

tion datasets. While the goal of this project is to study human activity as a driver of consumption rather than load disaggregation, building a tagged dataset of consumption and behavior would provide a means of evaluating load disaggregation methods with an additional degree of freedom.

Bibliography

[1] K. Moslehi and R. Kumar, "A reliability perspective of the smart grid," *Smart Grid, IEEE Transactions on*, vol. 1, no. 1, pp. 57–64, 2010.

[2] B. Jiang and Y. Fei, "Smart home in smart microgrid: A cost-effective energy ecosystem with intelligent hierarchical agents," *Smart Grid, IEEE Transactions on*, vol. 6, no. 1, pp. 3–13, 2015.

[3] R. Masiello, K. Vu, L. Deng, A. Abrams, K. Corfee, J. Harrison, KEMA, D. Hawkins, Y. Kunjal, and C. I. S. O. Corp., "Research evaluation of wind and solar generation, storage impact, and demand response on the california grid," California Energy Commission, Tech. Rep., 2010.

[4] C. E. Commission, "Renewable energy: California renewables portfolio standard program," California Energy Commission, Tech. Rep., 2002.

[5] ——, "Energy: renewable energy resources," June 30, 2011.

[6] R. Swearingen, "Research evaluation of wind and solar generation, storage impact, and demand response on the californa grid," California Energy Comission, Tech. Rep., 2010.

[7] N. Consulting, "Carbon dioxide reductions from demand response: Impacts in three markets," Navigant Consulting, Washington DC, Tech. Rep., November 2014.

[8] D. Watson, N. Matson, J. Page, S. Kiliccote, M. Piette (LBNL), K. Corfee, B. Seto, R. Masiello, J. Masiello, L. Molander, S. Golding, K. Sullivan, W. Johnson, D. Hawkins, and KEMA, "Fast automated demand response to enable the integration of renewable resources." California Energy Commission, Tech. Rep., 2012.

[9] U. E. I. Administration, "Energy perspectives 1949-2011," US Energy Information Administration, Tech. Rep., September 27 2011.

[10] United States Federal Energy Regulatory Comission, "A national assessment of demand response potential." Federal Energy Regulatory Comission, Tech. Rep., 2009. [Online]. Available: http://www.ferc.gov/legal/staff-reports/06-09-demand-response.pdf

[11] U.S. Energy Information Administration, "Drivers of U.S. household energy consumption, 1980-2009," February 2015. [Online]. Available: https://www.eia.gov/analysis/studies/buildings/households/

[12] N. D. Sintov and P. W. Schultz, "Unlocking the potential of smart grid technologies with behavioral science," *Frontiers in psychology*, vol. 6, 2015.

[13] J. Ma, H. H. Chen, L. Song, and Y. Li, "Residential load scheduling in smart grid: A cost efficiency perspective," *IEEE Transactions on Smart Grid*, vol. 7, no. 2, pp. 771–784, March 2016.

[14] M. A. A. Pedrasa, T. D. Spooner, and I. F. MacGill, "Coordinated scheduling of residential distributed energy resources to optimize smart home energy services," *IEEE Transactions on Smart Grid*, vol. 1, no. 2, pp. 134–143, Sept 2010.

[15] T. Logenthiran, D. Srinivasan, and T. Z. Shun, "Demand side management in smart grid using heuristic optimization," *IEEE Transactions on Smart Grid*, vol. 3, no. 3, pp. 1244–1252, Sept 2012.

[16] A. J. Conejo, J. M. Morales, and L. Baringo, "Real-time demand response model," *IEEE Transactions on Smart Grid*, vol. 1, no. 3, pp. 236–242, Dec 2010.

[17] M. Miozzo, D. Zordan, P. Dini, and M. Rossi, "Solarstat: Modeling photovoltaic sources through stochastic markov processes," in *2014 IEEE International Energy Conference (ENERGYCON)*. IEEE, 2014, pp. 688–695.

[18] A. Biason and M. Zorzi, "On the effects of battery imperfections in an energy harvesting device," in *Computing, Networking and Communications (ICNC), 2016 International Conference on*. IEEE, 2016, pp. 1–7.

[19] N. Dang, R. Valentini, E. Bozorgzadeh, M. Levorato, and N. Venkatasubramanian, "A unified stochastic model for energy management in solar-powered embedded systems," in *Proceedings of the IEEE/ACM International Conference on Computer-Aided Design*. IEEE Press, 2015, pp. 621–626.

[20] J. Goodman, "Stochastic calculus," University Lecture Notes, September 2011.

[21] H. G. Tucker, "Barebones background for Markov chains," University Lecture Notes, September 2006.

[22] R. J. Elliott, L. Aggoun, and J. B. Moore, *Hidden Markov models: estimation and control*. Springer Science & Business Media, 2008, vol. 29.

[23] E. Kim, S. Helal, and D. Cook, "Human activity recognition and pattern discovery," *Pervasive Computing, IEEE*, vol. 9, no. 1, pp. 48–53, 2010.

[24] M. F. Neuts, *Algorithmic probability: a collection of problems*. CRC Press, 1995, vol. 3.

[25] D. Blackwell, "Discrete dynamic programming," *The Annals of Mathematical Statistics*, vol. 33, no. 2, pp. 719–726, 1962. [Online]. Available: http://www.jstor.org/stable/2237546

[26] M. Geist, O. Pietquin, and G. Fricout, "Tracking in reinforcement learning," in *International Conference on Neural Information Processing*. Springer, 2009, pp. 502–511.

[27] J. M. Zacks and B. Tversky, "Event structure in perception and conception." *Psychological bulletin*, vol. 127, no. 1, p. 3, 2001.

[28] Bureau of Labor Statistics, "American time use survey," US Department of Labor, Tech. Rep., June 2015. [Online]. Available: https://www.bls.gov/tus

[29] N. Krishnan, D. J. Cook, and Z. Wemlinger, "Learning a taxonomy of predefined and discovered activity patterns," *Journal of ambient intelligence and smart environments*, vol. 5, no. 6, pp. 621–637, 2013.

[30] B. Aksanli, A. S. Akyurek, and T. S. Rosing, "User behavior modeling for estimating residential energy consumption," *EAI International Conference on Smart Grids for Smart Cities*, 2015.

[31] A.-H. Mohsenian-Rad, V. W. Wong, J. Jatskevich, R. Schober, and A. Leon-Garcia, "Autonomous demand-side management based on game-theoretic energy consumption scheduling for the future smart grid," *Smart Grid, IEEE Transactions on*, vol. 1, no. 3, pp. 320–331, 2010.

[32] T. Zia, D. Bruckner, and A. Zaidi, "A hidden markov model based procedure for identifying household electric loads," in *IECON 2011-37th Annual Conference on IEEE Industrial Electronics Society*. IEEE, 2011, pp. 3218–3223.

[33] "Solar cell i-v characteristic and the solar cell i-v curve," http://www.alternative-energy-tutorials.com/energy-articles/solar-cell-i-v-characteristic.html, 2016, accessed: 2017-05-30.

[34] M. Lichman, "UCI machine learning repository," 2013. [Online]. Available: http://archive.ics.uci.edu/ml

[35] E. Sage, "How to choose the best battery for a solar panel system," https://www.energysage.com/solar/solar-energy-storage/what-are-the-best-batteries-for-solar-panels/, accessed: 2017-05-13.

[36] S. Jensen, C. N. Rasmussen, and G. Y. (DTU), "White paper: 1.5 battery modeling," Edison: Electric Vehicles in a Distributed and Integrated Market Using Sustainable Energy and Open Networks, Rosenrns All 9, 1970 Frederiksberg Copenhagen, Denmark. T:+45 35 300 400, Tech. Rep. D1.5.1v1.1, 2009. [Online]. Available: http://www.edison-net.dk/~/media/EDISON/Reports/WP_1_5_Battery_Modelling_approvedx.ashx

[37] E. ASTM, "1049-85. 2005," *Rain flow counting method*, 1987.

[38] M. Matsuishi and T. Endo, "Fatigue of metals subjected to varying stress," *Japan Society of Mechanical Engineers, Fukuoka, Japan*, vol. 68, no. 2, pp. 37–40, 1968.

[39] I. Laresgoiti, S. Kbitz, M. Ecker, and D. U. Sauer, "Modeling mechanical degradation in lithium ion batteries during cycling: Solid electrolyte interphase fracture," *Journal of Power Sources*, vol. 300, pp. 112 – 122, 2015. [Online]. Available: http://www.sciencedirect.com/science/article/pii/S0378775315302949

[40] M. Miner *et al.*, "Cumulative fatigue damage," *Journal of applied mechanics*, vol. 12, no. 3, pp. A159–A164, 1945.

[41] D. P. Bertsekas, D. P. Bertsekas, D. P. Bertsekas, and D. P. Bertsekas, *Dynamic programming and optimal control*. Athena Scientific Belmont, MA, 1995, vol. 1, no. 2.

[42] M. Levorato, S. Narang, U. Mitra, and A. Ortega, "Reduced dimension policy iteration for wireless network control via multiscale analysis," in *IEEE Global Communications Conference (GLOBECOM), 2012*. IEEE, 2012, pp. 3886–3892.

[43] O. Parson, S. Ghosh, M. Weal, and A. Rogers, "An unsupervised training method for non-intrusive appliance load monitoring," *Artificial Intelligence*, vol. 217, pp. 1–19, 2014.